EXPERIMENTAL STUDY OF LAMINATED COMPOSITE TUBES UNDER BENDING

by

PUNEET SAGGAR

Presented to the Faculty of the Graduate School of

The University of Texas at Arlington in Partial Fulfillment

of the Requirements

for the Degree of

MASTER OF SCIENCE IN MATERIALS SCIENCE AND ENGINEERING

THE UNIVERSITY OF TEXAS AT ARLINGTON

May 2007

ACKNOWLEDGEMENTS

From core of my heart I would like to thank Dr. Wen S. Chan for his expert guidance and patience he displayed during the time period of my stay with him. His unique way of teaching was very precious to me and that's what helped me in building fundamentals in the field of composites.

I would like to thank Mr. Skip Pankewich and Mr. Mike Finn at United Sport Technologies, Inc. for supplying specimens needed for this study.

I would also like to thank Dr. Pranesh B. Aswath for his help that I needed regarding calibration and trouble shooting of the MTS machine.

I would like to extend my appreciation to Dr. Shashank Priya for serving as a committee member.

I would like to thank my father, brother, Dr. Guna Selvaduray and Santosh for the moral support they gave me all through in my Master's.

My sincere thanks to all my friends- Ramoun, Vaneet and Chethana for their much needed help they provided in various stages of research and documentation in this thesis.

April 16, 2007

ABSTRACT

EXPERIMENTAL STUDY OF LAMINATED

COMPOSITE TUBES UNDER BENDING

Publication No. _____

Puneet Saggar, M.S

The University of Texas at Arlington, 2007

Supervising Professor: Dr. Wen S. Chan

Bending stiffness of laminated composite tubes was determined experimentally using four-point bending test. The experimental results were compared with the results obtained by the laminated plate and smear property approaches. The results indicate that experimental values are closer to prediction of the laminated plate approach compared to smear property approach. Effects of tube radius and stacking sequence and fiber orientation of the walled thickness laminate on bending stiffness and strength of composite tubes were studied.

Fracture analysis was conducted to investigate the failure process of the tube. Both techniques of x-ray radiography and optical microscopy were used in this study. It is found that damage is initiated at the loading point. The failure process depends on the

fiber orientation and ply stacking sequence of the walled laminate of the tubes. The tubes finally failed in compression. Fiber breakage and delamination were observed as the prominent damage modes.

TABLE OF CONTENTS

ACKNOWLEDGMENTS iii

ABSTRACT iv

LIST OF ILLUSTRATIONS ix

LIST OF TABLES xi

Chapter

1. INTRODUCTION AND LITERATURE REVIEW 1

1.1 Composites and their advantages 1

1.2 Applications of composite tube(s) 1

1.3 Fabrication of composite tubes 2

1.4 Literature survey and previous work on composite tubes in bending 3

1.5 Objective and outline of this study 5

2. EXPERIMENTAL PROGRAM 7

2.1 Description of Test Plan 7

2.2 Characterization of principal material properties (E_1, E_2, G_{12}, ν_{12}) 7

2.2.1 Specimen preparation 8

2.2.2 Testing for basic material properties 11

2.3 Four-point bends testing of composite tubes 11

2.3.1 Geometry and lay-up of composite tubes 11

2.3.2 Fabrication of composite tube and inspection method 13

2.3.3 Test Fixture design and test set up 14

2.3.4 Specimen preparation 16

2.3.5 Test procedure 17

3. REVIEW OF ANALYTICAL MODELS FOR BENDING STIFFNESS EVALUATION OF COMPOSITE TUBES 18

3.1 Geometry and loading of composite tube 18

3.2 Lamination theory 19

3.2.1 Ply stress-strain relationships in material coordinates 19

3.2.2 Ply stress-strain relationships in laminate coordinates 20

3.2.3 Laminate constitutive equations 21

3.3 Laminated plate approach 22

3.4 MATHEMATICA Program 25

4. EXPERIMENTAL RESULTS 27

4.1 Test results and discussion of principal material properties 27

4.2 Strength of composite tube and their load-deflection curves 29

4.2.1 Sudden failure of composite tubes 30

4.2.2 Gradual failure of composite tubes 31

4.2.3 Effect of radius 32

4.2.4 Effect of 0˚ ply location 33

4.2.5 Effect of fiber orientation of angle plies 35

4.3 Curvature effect on bending stiffness of composite tube 36

4.3.1 Discussion for possible error in approaches 36

5. FAILURE INVESTIGATION..... 38

5.1 Failure Process and X-ray Radiography 38

5.1.1 X-ray radiographic procedure..... 39

5.1.2 Analysis of x-ray images 39

5.2 Optical Microscopic Analysis..... 44

5.2.1 Experimental Procedure..... 45

5.2.2. Delamination failure in tubes..... 46

6. CONCLUSIONS…….. 52

Appendix

A. MATHEMATICA CODE FOR STIFFNESS MATRICES… 55

REFERENCES 59

BIOGRAPHICAL INFORMATION..... 61

LIST OF ILLUSTRATIONS

Figure		Page
2.1	(a) 0° coupon (E_1 and ν_{12}), (b) 90° coupon (E_2), (c) 10° coupon (G_{12}), (d) side view of coupons	10
2.2	Geometry of the composite tube and section A-A´	12
2.3	Typical set up for four point bending test	15
2.4	Base plate for the fixture	16
2.5	Top plate attached to load cell	16
3.1	Infinitesimal section of composite tube	23
3.2	Flowchart for Bending Stiffness matrix computation of composite tube	26
4.1	Failed 0˚, 90˚ and 10˚ off-axis coupons	28
4.2	Load vs. Displacement for sudden failure specimens	30
4.3	Load vs. Displacement for 2C1 specimen	31
4.4	Load vs. Displacement for 2B2 specimen	32
4.5	Deflection vs. Load curves for various inner radii	33
4.6	Deflection vs. Load data on number of zero-degree plies	34
4.7	Effect of fiber orientation in symmetric lay-ups in Deflection vs. Load	35
4.8	2B3 specimen under four-point bending	37
5.1	X-ray image of specimen 2A1	40
5.2	X-ray image of specimen 2A2	41

5.3 X-ray image of specimen 2A3 41

5.4 X-ray image of specimen 2B1 42

5.5 X-ray image of specimen 2B2 43

5.6 X-ray image of specimen 2B3 43

5.7 X-ray image of specimen 2C1 44

5.8 X-ray image of specimen 2C2 44

5.9 Specimen for Optical Microscopy investigation 45

5.10 Fractured tube specimen 2A1 at 150X magnification 46

5.11 Fractured sample 2A2 at 70X magnification 47

5.12 Fractured sample 2A3 at 350X magnification 47

5.13 Specimen 2A2 at 100X magnification showing shear effect and failure between +45 and -45 plies 48

5.14 Specimen 2A3 at 300X magnification showing disastrous shear failure in the middle 49

5.15 Specimen 2A1 at 275X showing delamination and crack-propagation in oblique manner from layer to layer as well 49

5.16 Crack propagation in 2A3 at 350X magnification 50

5.17 Failed sample 2B1 at 200X magnification showing crack propagation 50

5.18 Failed sample 2C1 at 100X showing delamination and crack propagation from layer to layer as well 51

LIST OF TABLES

Table Page

2.1. Test Plan for determination of material properties 8

2.2 Lay-up and radius of specimens 13

2.3 Effects studied by lay-ups 13

4.1 Material property test data 28

4.2 Failure load and first damage load of tube specimens 29

4.3 Bending stiffness of various lay-ups of composite tubes 36

CHAPTER 1

INTRODUCTION AND LITERATURE REVIEW

1.1 Composites and their advantages

A composite by general definition means a combination of two or more materials combined together in such a way that it gives better properties than the individual material system in it. Structural composites are a blend of two or more components, one of which is stiff, long fibers and the other, a binder or 'matrix' which holds the fibers in place. Fibers are usually much stronger than the matrix material. When fibers and matrix are joined to form composite they retain their identities but both directly influence composite's final properties. Due to the high strength and load bearing capacity possessed by fibers (reinforcement phase), composite usually exhibits better mechanical properties in the direction of fibers. So a structural fiber reinforced composite is a layered structure having fiber orientation in each layer designed to get maximum benefit in different directions for desired application. These advantages are not just tamed by aircraft industry but also in everyday use of golf shafts and tennis rackets.

1.2 Applications of composite tube(s)

For the lucrative benefits of high specific strength and high specific stiffness offered by fiber reinforced composites, they are put into wide variety of applications. Until 1991 about 10% of the money invested in advanced composites used to come

from sports industry [1]. But slowly there has been active use of composites in most industries and now the arena is not just limited to defense sector only. Composite tubes found their application in golf shafts. Composites in rolled or tubular form are used by printing industry a lot these days. Being light and strong the printer rollers retain their strength but light weight gives them benefit in print quality than steel rollers and also lesser vibrations. Composite tubes with uniform circular cross-section or tapered cross-sections find use in drive shafts because of extra stiffness, they get higher whirling speeds. Very stiff shafts for lathe, very strong for trucks and well insulated shafts for trolley buses and generators are some applications where composite tubes are put into. Tubes with square cross-section are being used for robotic applications where light weight of robot enhances its performance speed and extra stiffness adds to its mechanical properties.

1.3 Fabrication of composite tubes

Composite tubes can be fabricated in several ways, namely- filament winding, pre-preg rolling (sheet wrapping) and pultrusion. These techniques can be utilized either directly or indirectly to aid in tube construction. Choice of technique is dominated by properties required, cost and quantity. Of the four types of methods listed, filament winding is the most common for tubes.

Pre-preg rolling is the most popular method. In this technique, layers of material are rolled around a mandrel, by hand or machine, prior to consolidation or cure. This process is ideal for smaller quantities and smaller tubes where increased material costs

are less significant. This technique is adopted in this study and will be explained in more detail in chapter 2.

Pultrusion is a continuous process in which fibers in form of roving, mat or fabric are impregnated with resin and pulled through a heated die of the required shape, molding through the inside and outside diameters. This technique uses raw materials in their most basic forms and lowest cost forms. Due to high tooling cost, large quantities need to be produced to make this process cost effective. The main drawback of this method is the choice of fiber angle is very limited.

Circular cross-sections are typical of filament winding with an added advantage of several fiber angles and shapes. On the other hand, it can create high fiber volume fraction parts with high quality as well. In this process, fiber bundles, after impregnating with resin, are wound on mandrel ate the angle required to produce the mechanical properties as well. Fibers can be positioned at any angle within the tube, with different layers at different angles to carry the various internal and external loads applied. Tubes are seldom made of pure 0˚ or pure 90˚ fibers as they would easily split. Tubes produced in this way, have a molded inside diameter and outside diameter can be machined if required, after curing.

1.4 Literature survey and previous work on composite tubes in bending

Considerable efforts have been conducted in studying properties of composite laminated beams in bending. Beams with I-section and hat-section under bending been studied. Increasing use of composites in civil structures and sporting goods, various sizes of composite tubes have attracted many interests in understanding their structures

response. Fam and Rizkalla [2] studied large diameter glass-fiber reinforced polymer (GFRP) under bending to see the effects of concrete filling, central hole, and laminate structure for strength to weight ratio and ductility of the tubes. Reddy and Binienda [3] explained the bending phenomena in composite beams by new theory which includes anisotropic nature of composites. Taheri et al. [4] carried out comprehensive numerical investigation to evaluate the response and energy absorption capacity of hybrid composite tubes made of unidirectional pultruded tube over wrapped with ±45° fiber reinforced plastic. Parametric studies conducted examined the effect of tube's length, thickness and type of braid and loading conditions as well on crushing behavior of the tubes. Chan and Demirhan [5] evaluated bending stiffness of composite tubes using the modified lamination theory of composites. In their approach, change of fiber orientation along the circumference of the tube is included. Hu et al [6], using numerical analysis, evaluated macroscopic properties under biaxial bending of thin walled composite tube. Stockwell and Cooper [7] investigated collapsing behavior of moderate wall thickness composite tubes by finite element analysis. Padmanabhan et al.[8] examined the mechanical behavior of an AlSiC metal matrix composite tubular samples with 17.8% of volume fraction of 3μm SiC particles in a 2124 aluminum matrix. The tubes were under ratios of combined tension and torsional loads. Grediac et al. [9] presented a method to determine the four principal material constants of the through-thicknesses of thick laminated composite tube. Ellyin and Maser [10] investigated the effects of moisture absorption and exposure to elevated temperature on the mechanical properties of glass fiber reinforced epoxy filament wound composite tubes. They performed multi-

axial tests and observed that for all biaxial stress ratios, strength and stiffness decreased to some extent with presence of moisture and elevating the temperature. Nixon [11] determined twist deformations for the design of full-scale extension-twist coupled tilt-rotor blades by conducting static torsion and axial tension tests on extension-twist-coupled circular tubes. Chen et al. [12] experimentally investigated the impact damage tolerance of thin walled composite struts made of both brittle and toughened epoxy. They used two different impactor sizes and evaluated damage parameters like barely visible surface damage, internal damage and residual strength against impact energy. Krafchak et al. [13] presented experimental results to assess the effects of barely visible internal damage on fatigue life of thin walled composite tubes. Undamaged composite tubes and impact damaged composite tubes were tested in compression-compression fatigue and they observed that fatigue life degraded because of impact damage. Barely visible impact damage was predominantly due to matrix cracking and delamination in their study. Jensen and Pickenheim [14] identified failure mechanisms and measured compressive strength and stiffness of specimens that modeled micro modulations as their focus was to determine compressive performance of a filament-wound cylinders.

1.5 Objective and outline of this study

After reviewing the past work in composite tubes, little work has been conducted in evaluating the bending stiffness of composite tubes. Accurate evaluation of bending stiffness is important for better prediction of deflection, buckling loads and vibration response of structures. The purpose of this research was to experimentally evaluate bending stiffness of uniform diameter composite tube. Four-point bending tests

are conducted using MTS machine. Chapter 2 mainly discusses the experimental test plan and testing procedures in detail that were used in this study.

Chapter 3 reviews analytical model for evaluation of the bending stiffness of composite tubes. A MATHEMATICA program is developed based on this model. Chapter 4 presents and discusses the results obtained by tests. Chapter 5 investigates the failure process of composite tube under bending by using x-ray radiograph and optical fractography methods. The conclusions of this study are summarized in chapter 6.

CHAPTER 2

EXPERIMENTAL PROGRAM

This chapter covers test plan devised to obtain principal material properties of material and the bending stiffness of the tube. The experimental program also aims to evaluate the effect of bending stiffness and bending strength due to stacking sequence, fiber orientation and radius of the tube.

2.1 Description of Test Plan

Four point bending was primarily used as a test method to evaluate bending stiffness of composite tubes. The whole test program was divided into two parts. Part one was related to evaluate the material properties needed to incorporate in the calculation of bending stiffness by analytical methods. Part two was mainly to obtain data from strain gage and dial gage to assess the bending stiffness of the tubes.

2.2 Characterization of principal material properties (E_1, E_2, G_{12}, υ_{12})

Determination of material properties is very important to evaluate bending stiffness of composite tubes. For a thin layer of composite material, four basic material constants are required to fully characterize the material structural response. They are elastic modulus along the fiber, E_1, along the transverse fiber direction, E_2, shear modulus in the plane, G_{12} and the Poisson's ratio, υ_{12}. These four constants were evaluated using the specifications as per ASTM standards. Table 2.1 lists the typical specimen sizes, specimen type and the ASTM standard specifications that were used for

each test. As indicated in Table 2.1, no ASTM standard specification was adopted for determining the shear modulus in this study. In measuring shear modulus of fiber reinforced composites, ASTM D4255 standard specification is often used. In this specification, picture-frame or rail-shear fixture is needed. In this study, a 10˚ off-axis tension test is used. This test is simple and requires no special fixture. This test has been often used by industries.

Table 2.1 Test Plan for determination of material properties

Specimen type	Specimen dimension	No. of plies	Material property determined	ASTM standard specification
0˚ coupons	0.5″ X10.0″	5	E_1 and υ_{12}	D3039/D3039M-00(2006)
90˚ coupons	1.5″ X 10.0″	10	E_2	D3039/D3039M-00(2006)
10˚ coupons	1.0″ X 10.0″	5	G_{12}	NONE

2.2.1 Specimen preparation

Composite panels were made by T700S/G91 graphite/epoxy prepreg. The panels were cured at 270 F and manufactured by Sawyer Composites in Fort Worth, Texas. As per the ASTM standard-D3039/D3039M-00(2006) described in Table 2.1, required coupons were made of unidirectional reinforced composite and these coupons were tested in MTS machine to generate the data which was then assimilated to evaluate the material properties. The following procedures were adopted and specimens were made ready to be tested.

1. Cut the cured panels into desired dimensions specified in Table 2.1.
2. Attach aluminum end tabs on each coupon using two-part epoxy adhesive.
3. Measure the width and thickness of each coupon in the test zone at three different locations.
4. Attach strain gage(s) on each coupon using epoxy solution giving adequate curing time to ensure perfect bond between gage and specimen.

Figure 2.1 shows dimensions and gage locations of different coupons used to obtain all of the principal material properties.

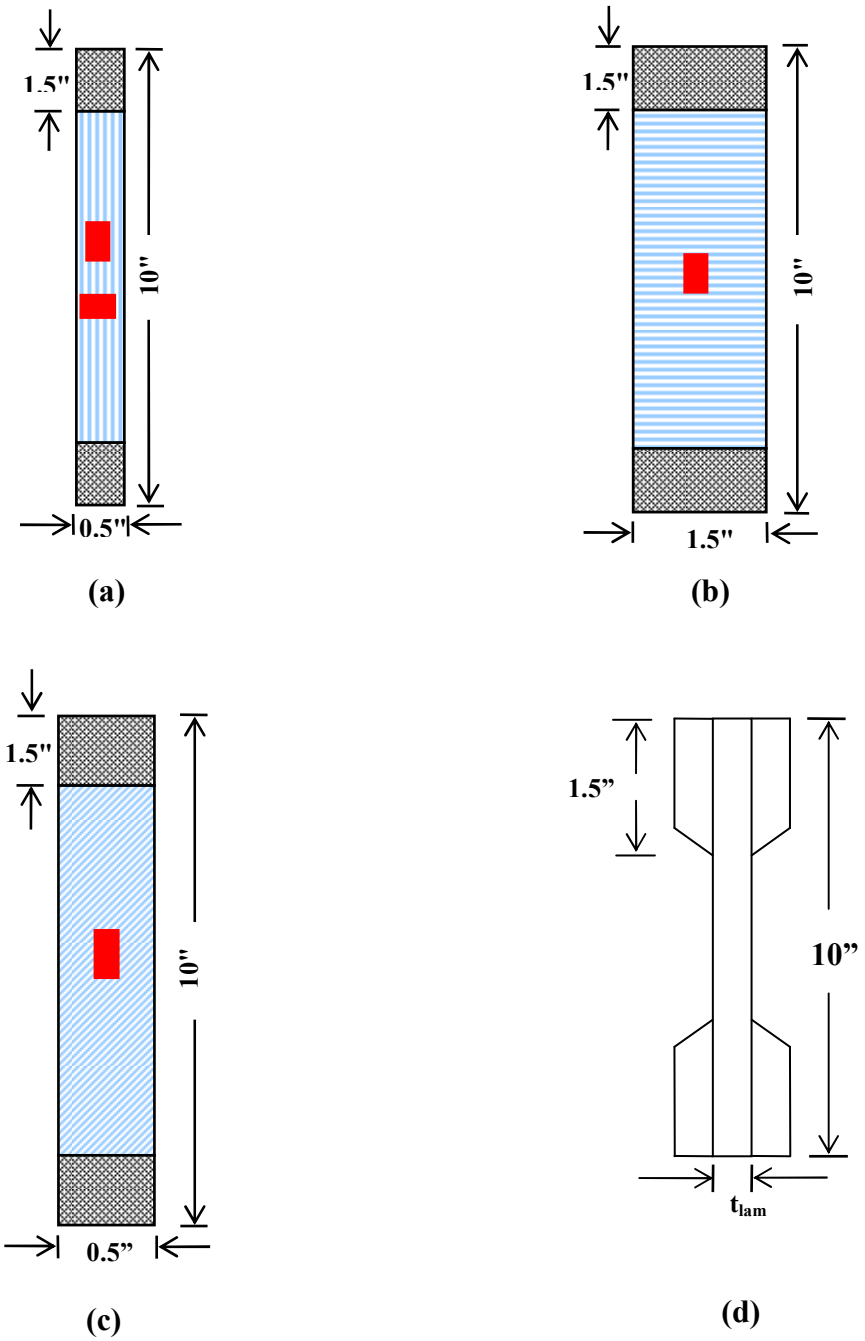

Figure 2.1 (a) 0˚ coupon (E_1 and υ_{12}), (b) 90˚ coupon (E_2), (c) 10˚coupon (G_{12}), (d) side view of coupons.

2.2.2 Testing for basic material properties

The MTS machine was calibrated on its 10KN load cell first. The test specimen was properly placed in the grip. The load is applied at a rate of 0.02 inches per minute. During the loading, the loads and their corresponding displacements and strain data were recorded through the data acquisition system. Strain gage data were only obtained at a prescribed load interval. During loading specimens are observed visually with aid of magnifying lens for any damage that may occur. The specimens were loaded until total failure.

2.3 Four-point bending test of composite tubes

Flexural behavior of structural composites is characterized by bending test. Two types of bending tests are usually used, namely three-point bending test and four-point bending tests. In the three-point bending test, the moment along the specimen length is linear and reaches the maximum at the loading point. In this case, the transverse shear along the specimen length is constant between the loading and supported points. This test is often used to study the transverse shear behavior of the composites. In the four-point bending test, the bending moment between two loading points of the specimen is a constant. This provides a convenient way to evaluate the bending stiffness of the test sample. Bending stiffness of the uniform cross-section circular composite tubes is evaluated by this test.

2.3.1 Geometry and lay-up of composite tubes

Table 2.2 lists the laminate lay-up of tubular wall, radius and number of the test specimens. Four different radii of the composite tubes, R=0.25, 0.375, 0.5 and 0.75 inch

with the identical lay up of walled laminates were used to investigate the effect of radius on the bending stiffness of the tube.

For R=0.375 inch, a set of $[0/-45/+45]_S$ with different stacking sequences were used to study the bending stiffness and their failure process. Laminates with $[0/-15/+15/+15/-15/0]_T$, $[0/-45/+45/+45/-45/0]_T$ and $[0/-75/+75/+75/-75/0]_T$ were used to investigate the effect of fiber orientation on bending stiffness and strength of composite tube under bending.

Table 2.3 tabulates the lay-ups that are used for effects studied.

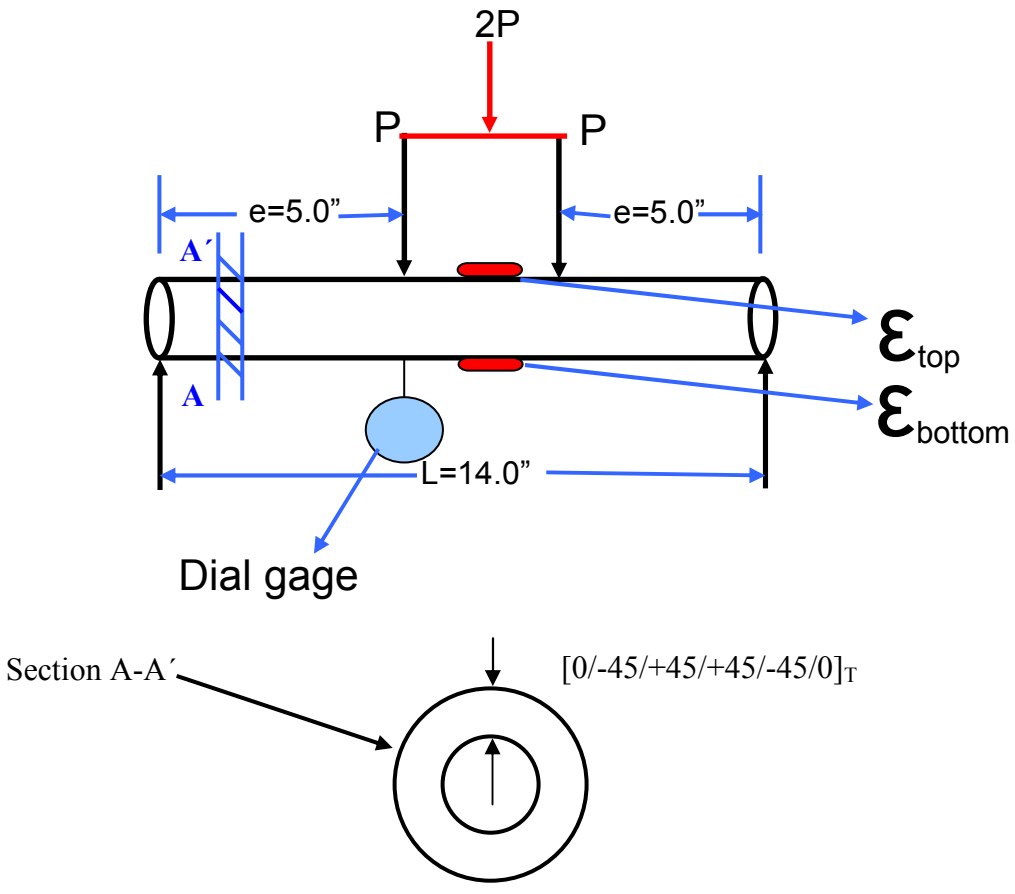

Figure 2.2 Geometry of the composite tube and section A-A´.

Table 2.2 Lay-up and radius of specimens

Specimen type	Lay-up	Inner radius (in)
2A1	$[0/-45/+45/+45/-45/0]_T$	0.375
2A2	$[-45/+45/0/-45/+45/0]_T$	0.375
2A3	$[0/0/+45/-45/+45/-45]_T$	0.375
2B1	$[0/-45/+45/+45/-45/0]_T$	0.25
2B2	$[0/-45/+45/+45/-45/0]_T$	0.5
2B3	$[0/-45/+45/+45/-45/0]_T$	0.95
2C1	$[0/-15/+15/+15/-15/0]_T$	0.375
2C2	$[0/-75/+75/+75/-75/0]_T$	0.375

Table 2.3 Effects studied by lay-ups

Effect studied	Lay-up(s) used
Stacking sequence	2A1, 2A2, 2A3
Radius	2B1, 2A1, 2B2, 2B3
Fiber orientation	2A1, 2C1, 2C2

2.3.2 Fabrication of composite tube and inspection method

In general composite tubes can be fabricated by several different ways. Sheet-wrapping, filament winding and pultrusion are among the popular methods to manufacture the composite tubes. The composite tube specimens were supplied by United Sports Technologies. The tubes were manufactured by sheet-wrapping process in which the unidirectional fiber-reinforced prepregs were hand laid and then machine rolled on steel mandrel. To apply pressure from outside poly-propylene tape was used and steel mandrel gave it pressure from inside while curing. Curing temperature for the material chosen is 270 F and curing cycle for the same is 70 minutes. The tubes were cured in oven vertically.

The main advantage of this process over filament winding is its ability to lay prepregs at desired angle. Another most common procedure to fabricate uniform circular tube is by pultrusion in which constant cross-section area is the main requirement.

After the tubes were fabricated, they were inspected visually to see any damages or initial curvature induced. As the tubes were hung vertically during curing, the induced curvature of the tubes was minimal. Any surface cracks were inspected visually using paper paint.

2.3.3 Test Fixture design and test set up

Figure 2.2 shows the tube geometries and a typical lay-up of composite tube. As shown in the figure, the distance between the two fixed plates is 14 inches and composite tube is 18 inches in length with 2 inches of hanging length on either side was given. The composite tube is placed on fixture which was designed for this experiment and loaded until failure to record for deflection and strain at specified locations. In order to perform the four-point bending test fixture was designed so that the test set-up can allow to measure data needed for calculations. A typical set up for four-point bending test is shown in Figures 2.3.

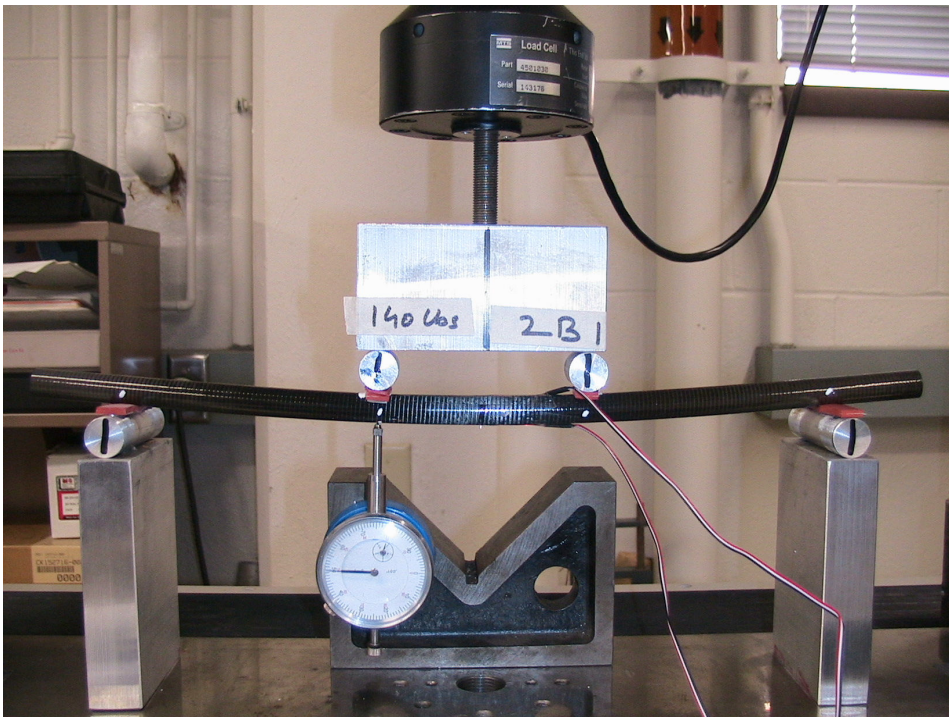

Figure 2.3 Typical set up for four-point bending test.

On the base of the machine were designed two aluminum plates screwed inside firmly with roller supports on top. The point pin support allows the tube free rotated and gives no additional moment to the tube. Figure 2.4 shows the detail of the base plate. Upper plate shown in Figure 2.5 was designed to screw into 10 KN capacity load cell with two rollers on either ends which are 4 inches apart. The test load was applied to the composite tube through these rollers. To avoid sudden failure at upper loading pins a firm polymeric cushion was attached on the rollers. Test runs were performed to select right thickness of cushion.

A dial gage (see Figure 2.3) was used to obtain deflection right below loading point. The gage was calibrated to obtain maximum deflection in the center of the tube to obtain bending stiffness. The strain gage was also used to record strain in tube during

loading. Two strain gages were mounted along the longitudinal direction on the top and bottom surfaces of the tube. During testing important observations were noted down carefully to evaluate the behavior which is of certain importance during their failure analysis.

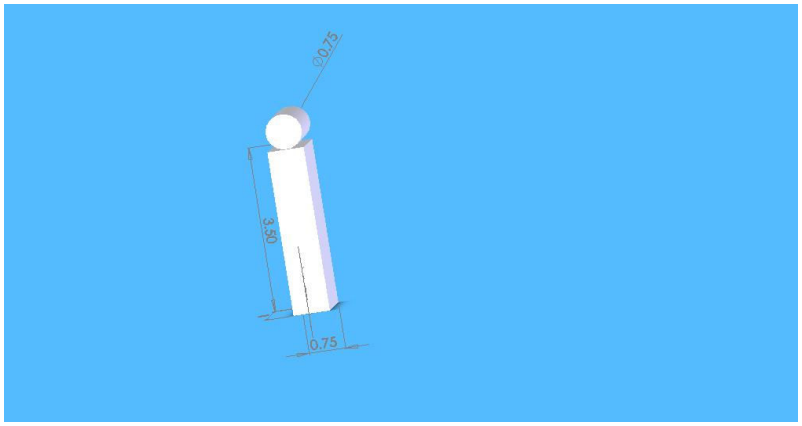

Figure 2.4 Base plate for the fixture.

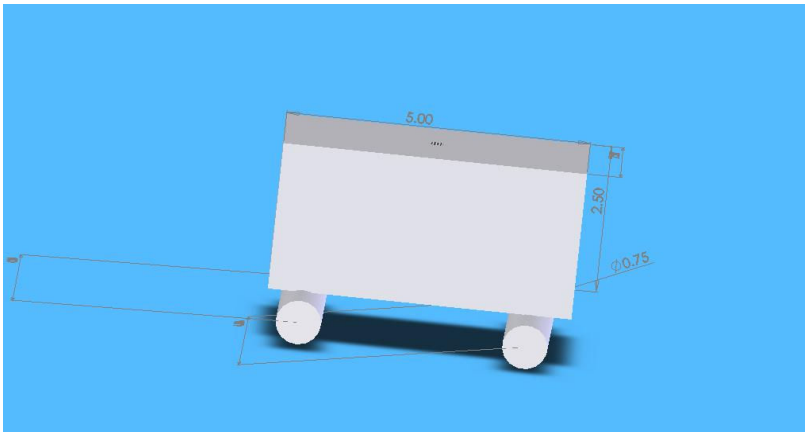

Figure 2.5 Top plate attached to load cell.

2.3.4 Specimen preparation

1. Measure the inner and outer diameter at 4 different locations to obtain wall thickness of the tube.
2. Inspect the test specimen for any damage that may occur during handling.

3. Mount strain gage along the longitudinal direction on the top and bottom surfaces of the test tube.
4. Mount strain gage using two part adhesive solution mentioned for the strain gage type and allow it to cure for required time span to get perfect bonding.

2.3.5 Test procedure

1. Place the test tube in the proper position on the fixture.
2. Both upper pins are in perfect contact with the tube.
3. Calibrate the 10KN load cell along with other data acquisition devices like dial gage and strain gage indicator for accurate results.
4. Load the tube at loading rate of 0.02 inches/min.
5. Set the zero reading of dial gage indicator and strain gage indicator before the load application.
6. Record strain gage and dial gage reading at the pre-set intervals.
7. Any peculiar behavior is recorded and cracking behavior on loading is important to observe and document and specimen is preserved at its fractured regions for its failure analysis under microscope.
8. Test is stopped when the tube fails or no longer carry the load.

CHAPTER 3

REVIEW OF ANALYTICAL MODELS FOR BENDING STIFFNESS EVALUATION OF COMPOSITE TUBES

In this chapter analytical model for calculating bending stiffness of uniform circular composite tube is reviewed. In evaluating bending stiffness of laminated composite tube, two approaches were often considered, one with using smear property approach. Both approaches employed lamination theory to calculate the properties of the laminate. A brief description of these approaches is included in this chapter.

3.1 Geometry and loading of composite tube

The composite tube considered here has a uniform circular cross-section with a radius R. R is measured from the center of the tube to the mid-plane of the wall-thickness. The length of the tube is much larger as compared to its radius. The tube is a layer structured with plies oriented in preferred orientations. The wall laminate of the tube can be in any general lay-up. The tube is subjected to pure bending moment, M_x. It should be noted that unlike the conventional strength of material, Mx points to the transverse to the longitudinal direction of the tube (x-direction). Mx is the resultant moment due to σ_x. It is assumed that plane cross-section remains plane and the circular cross-section remains unchanged after the deformation.

3.2 Lamination theory

A laminate contains multiple layers in different fiber orientations perfectly bonded together. To analyze this kind of laminate, an equivalent plate theory is developed. It is so-called laminated plate theory or lamination theory. The lamination theory is used to calculate the stresses and strains in different plies of laminated composite under load. It consists of a collection of mechanics-of-materials type of stress and deformation hypothesis which is described in this section. Using this theory, we proceed from basic building blocks, the lamina, to structural laminate. It is used to calculate the following terms:

- Stiffness matrices for the laminate
- Mid-plane strains and curvatures for each lamina
- In-plane stresses and strains for each laminas

Since the laminate is thin compared to other dimensions, the theory of plate is adopted. Because of thin lamina, the plane stress condition is assumed. That is,

$$\sigma_z = \tau_{xz} = \tau_{yz} = 0$$

3.2.1 Ply stress-strain relationships in material coordinates

The stress-strain relation for the orthotropic plies under plane stress can be expressed in terms of four independent elastic parameters, Q_{11}, Q_{12}, Q_{22} and Q_{66} as:

$$\begin{pmatrix} \sigma_1 \\ \sigma_2 \\ \tau_{12} \end{pmatrix} = \begin{pmatrix} Q_{11} & Q_{12} & 0 \\ Q_{21} & Q_{22} & 0 \\ 0 & 0 & Q_{66} \end{pmatrix} \begin{pmatrix} \varepsilon_1 \\ \varepsilon_2 \\ \gamma_{12} \end{pmatrix} \quad \text{Or} \quad [\sigma_{1-2}] = [Q_{1-2}][\varepsilon_{1-2}] \tag{3.1}$$

The subscripts 1, 2 and 6 refer to the principal coordinate system that is along the fiber, transverse to the fiber and shear direction, respectively. The components of the [Q] matrix is given as

$$Q_{11}=\frac{E_1}{1-\nu_{12}\nu_{21}}$$

$$Q_{22}=\frac{E_2}{1-\nu_{12}\nu_{21}} \tag{3.2}$$

$$Q_{21}=Q_{12}=\frac{E_1\nu_{21}}{1-\nu_{12}\nu_{21}}=\frac{E_2\nu_{12}}{1-\nu_{12}\nu_{21}}$$

$$Q_{66}=G_{12}$$

Where, E_1 and E_2 are the moduli of lamina along the fiber and transverse direction respectively. G_{12} is the shear modulus of lamina in 1-2 planes and ν_{12} is the Poisson's ratio of lamina due to the loading along the fiber direction.

3.2.2 Ply stress-strain relationships in laminate coordinates

Each layer in the laminate has its own principal material coordinate system. A coordinate system, x-y-z common to all of laminas is selected. These coordinates are usually set at the mid-plane of the laminate. The strains in any given lamina (k^{th} lamina) can be expressed in terms of strain at the mid-plane and the curvature of the laminate as follows:

$$\begin{Bmatrix}\varepsilon_x\\ \varepsilon_y\\ \gamma_s\end{Bmatrix}=\begin{Bmatrix}\varepsilon_x^{\circ}\\ \varepsilon_y^{\circ}\\ \gamma_s^{\circ}\end{Bmatrix}+z\begin{Bmatrix}\kappa_x\\ \kappa_y\\ \kappa_s\end{Bmatrix} \tag{3.3}$$

$$\begin{bmatrix}\sigma_x\\ \sigma_y\\ \tau_s\end{bmatrix}_k = \begin{bmatrix}Q_{xx} & Q_{xy} & Q_{xs}\\ Q_{yx} & Q_{yy} & Q_{ys}\\ Q_{sx} & Q_{sy} & Q_{ss}\end{bmatrix}_k \begin{bmatrix}\varepsilon_x^\circ\\ \varepsilon_y^\circ\\ \gamma_s^\circ\end{bmatrix} + z\begin{bmatrix}Q_{xx} & Q_{xy} & Q_{xs}\\ Q_{yx} & Q_{yy} & Q_{ys}\\ Q_{sx} & Q_{sy} & Q_{ss}\end{bmatrix}_k \begin{bmatrix}\kappa_x\\ \kappa_y\\ \kappa_s\end{bmatrix} \tag{3.4}$$

$[Q_{x\text{-}y}]_k$ is the stiffness matrix of the k^{th} lamina referred to the laminate coordinate system, x-y-z.

3.2.3 Laminate constitutive equations

The resultant forces, [N] and moments, [M] of the laminate can be obtained by:

$$[N] = \sum_{k=1}^{n} \int_{z_{k-1}}^{z_k} [\sigma]_k .dz$$

$$[M] = \sum_{k=1}^{n} \int_{z_{k-1}}^{z_k} [\sigma]_k .z.dz \tag{3.5}$$

After performing the integration, we have:

$$\begin{bmatrix}N\\ M\end{bmatrix} = \begin{bmatrix}A & B\\ B & D\end{bmatrix} . \begin{bmatrix}\varepsilon^\circ\\ \kappa\end{bmatrix} \tag{3.6}$$

Where,

$$[A] = \sum_{k=1}^{n} [\hat{Q}]_k \left(z_k - z_{k-1}\right)$$

$$[B] = \frac{1}{2}\sum_{k=1}^{n} [\hat{Q}]_k \left(z_k^2 - z_{k-1}^2\right) \tag{3.7}$$

$$[D] = \frac{1}{3}\sum_{k=1}^{n} [\hat{Q}]_k \left(z_k^3 - z_{k-1}^3\right)$$

z_k refers to the z coordinate of the upper interface of the k^{th} laminate. $[\hat{Q}]_k$ matrix is so- called reduced stiffness matrix of the k^{th} layer. The matrices, A, B and D are 3x3 matrices. They refer as extensional, extensional-bending coupling and bending stiffness matrices, respectively. Equation 3.6 is often called as "Laminate Constitutive Equations".

3.3 Laminated plate approach

The determination of bending stiffness for composite tubes by laminated plate approach was developed by Chan and Demirhan [5]. In their approach, an infinitesimal plate section of the tube laminate is considered as shown in Figure 3.1. This section has its axis x-y-z and is inclined at an angle θ with respect to axis of the composite tube. The plate section is rotated about x to position parallel to the y′-axis. The stiffness of the plate calculated by the lamination theory is translated to the axis y′ according to parallel axis theorem. The overall stiffness of the composite tube is then obtained by integrating over the entire θ domain.

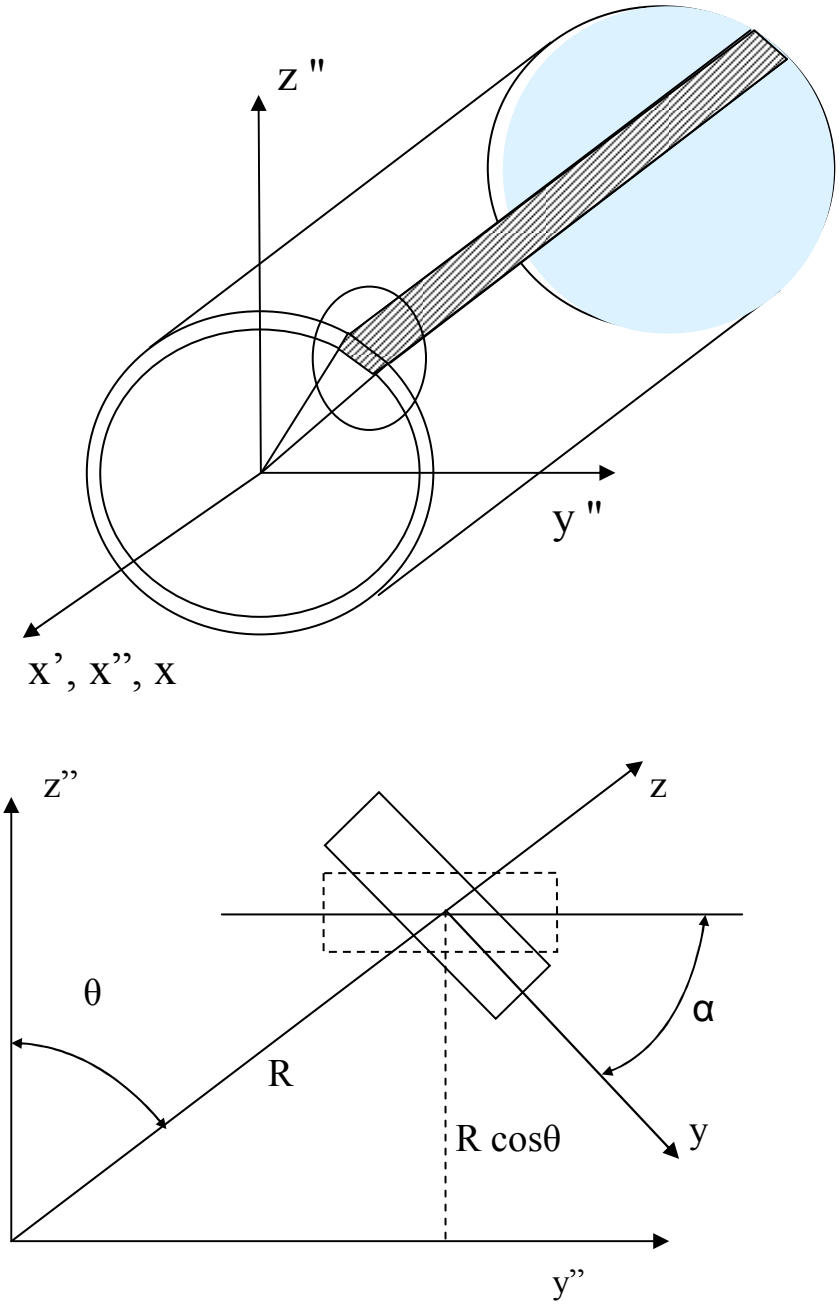

Figure 3.1 Infinitesimal section of composite tube.

The overall stiffness matrices, $\left[\overline{A}\right], \left[\overline{B}\right], \left[\overline{D}\right]$ of the tube can be expressed as:

$$\left[\overline{A}\right] = \int_0^{2\pi} \left[A'\right].R.d\theta$$

$$\left[\overline{B}\right] = \int_0^{2\pi} \left[B'\right].R.d\theta$$

$$\left[\overline{D}\right] = \int_0^{2\pi} \left[D'\right].R.d\theta$$

Where,

$$\left[A^{'}\right] = \left[A\right]$$

$$\left[B^{'}\right] = \left[B\right] + R.\cos\theta.\left[A\right]$$

$$\left[D^{'}\right] = \left[D\right] + 2R.\cos\theta.\left[B\right] + \left(R.\cos\theta\right)^2\left[A\right] \tag{3.8}$$

The [A′], [B′], [D′] matrices are the universal stiffness matrices per unit section of the composite plate as shown in figure with respect to x-y-z axis shown. Substituting equations and rearranging equations gives the final equations for calculation of the total extensional, coupling and bending stiffness matrices as follows:

$$\overline{A}_{ij} = \int_0^{2\pi}\left(\sum_{k=1}^{n} \hat{Q}_{ij}^{k}\left(z_k - z_{k-1}\right)\right).R.d\theta = R.\sum_{k=1}^{n}\left(\int_0^{2\pi} \hat{Q}_{ij}^{k}.d\theta\right)\left(z_k - z_{k-1}\right)$$

$$\overline{B}_{ij} = \frac{R}{2}\sum_{k=1}^{n}\left(\int_0^{2\pi} \hat{Q}_{ij}^{k}.d\theta\right)\left(z_k^2 - z_{k-1}^2\right) \tag{3.9}$$

$$\overline{D}_{ij} = \frac{R}{3}\sum_{k=1}^{n}\left(\int_0^{2\pi} \hat{Q}_{ij}^{k}\, d\theta\right).\left(z_k^3 - z_{k-1}^3\right) + R^3\sum_{k=1}^{n}\left(\int_0^{2\pi} \hat{Q}_{ij}^{k}.\cos^2\theta.d\theta\right)\left(z_k - z_{k-1}\right)$$

$\hat{Q}_{ij}^{k}$ is a function of rotation angle about x-axis, θ, fiber orientation angle, β, and the elastic material constants as shown in appendix.

The effective bending stiffness of the composite tube can be expressed as:-

$$D_x = \frac{1}{\overline{d}_{11}} \tag{3.10}$$

where $\overline{d}_{11}$ is the (4, 4) element of the inverse matrix of $\begin{bmatrix}\overline{A} & \overline{B} & \overline{D}\end{bmatrix}$ as shown as

$$\begin{bmatrix}\overline{a} & \overline{b} \\ \overline{b^T} & \overline{d}\end{bmatrix} = \begin{bmatrix}\overline{A} & \overline{B} \\ \overline{B} & \overline{D}\end{bmatrix}^{-1} \tag{3.11}$$

3.4 MATHEMATICA Program

In order to have efficient calculations on a public available software program, MATHEMATICA was used to resolve the equations used in laminated plate approach to get the value of bending stiffness. Features of this program include solving mathematical equations using constants and variables. Variables are assigned as functions in this program and there are certain codes which are followed to achieve the task to be done like integration, differentiation and solving complex equations as well in matrix form for this typical example. In this program, equations are input in certain format which is similar to programming language and program then calculates when it is run. The program coded for approach used in this work is described in flow chart shown in Figure 3.2 and detailed code is shown in appendix A.

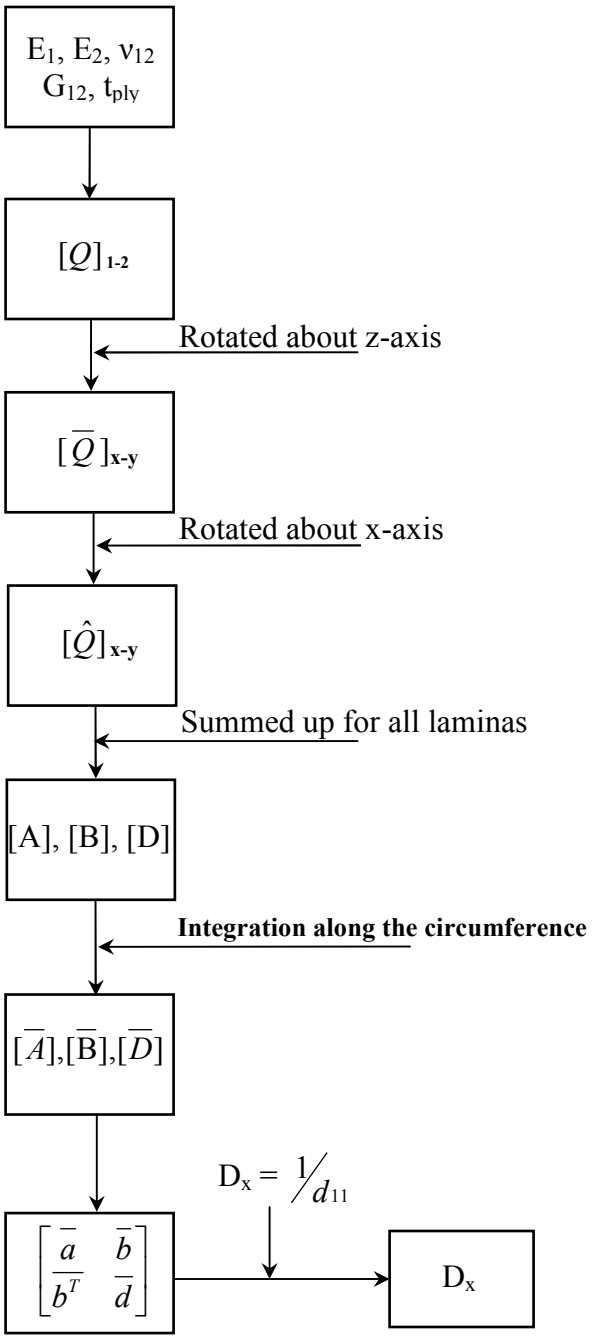

Figure 3.2 Flowchart for Bending Stiffness matrix computation of composite tube

CHAPTER 4

EXPERIMENTAL RESULTS

4.1 Test results and discussion of principal material properties

The principal material properties of lamina, E_1, E_2, υ_{12} and G_{12} are measured in this section. The thickness of the cured lamina is often considered a principal material property since it depends on cured process and relates to the fiber volume fraction. E_1 and E_2 are directly obtained from the slope of the stress-strain curves of 0˚ and 90˚ coupons, respectively (see equation 4.1). The stress-strain curve is constructed from the load-strain data which was stored in data acquisition system during the test. Poisson ratio was estimated from strain readings read by horizontal and vertical strain gages attached on zero-degree coupons (see equation 4.2). A 10˚ off axis coupon under tension test is used to measure the shear modulus of 0˚ lamina. Shear modulus (G_{12}) was calculated by using equation 4.3. In equation 4.3, E_x is obtained from the 10˚ coupon test. E_1, E_2 and υ_{12} in the right hand side of equation 4.3 is obtained from 0˚ and 90˚ coupon test data.

$$E_1 = E_2 = E_x = \frac{\Delta\sigma}{\Delta\varepsilon} \tag{4.1}$$

$$\nu_{12} = -\frac{\varepsilon_{lateral}}{\varepsilon_{longitudinal}} \tag{4.2}$$

$$\frac{1}{E_x} = \frac{m^2}{E_1}(m^2 - n^2\nu_{12}) + \frac{n^2}{E_2}(n^2 - m^2\nu_{21}) + \frac{m^2n^2}{G_{12}} \tag{4.3}$$

Here, m= cos10˚, n= sin10˚ and $\nu_{21} = \nu_{12}.\frac{E_2}{E_1}$

Table 4.1 lists the material properties of the lamina. The cured ply thickness is obtained by average measuring thickness of each coupon at three locations divided by number of plies in that coupon.

Table 4.1 Material property test data

Property Tested	Test Data	Average Numbers
E_1 (msi)	20.0, 20.5, 19.8	20.1
E_2 (msi)	1.77, 1.79, 1.76	1.77
G_{12} (msi)	1.1, 1.13, 1.1	1.11
υ_{12}	0.313	0.313
t_{ply} (inch)	0.0058	0.0058

Figure 4.1 shows images of broken 0˚, 90˚ and 10˚ off axis coupon, respectively.

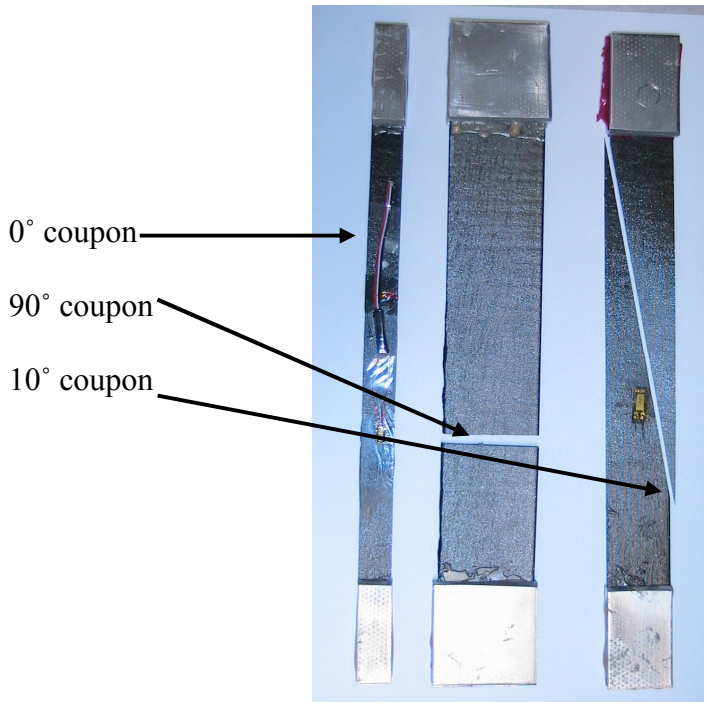

Figure 4.1 Failed 0˚, 90˚ and 10˚ off-axis coupons.

4.2 Strength of composite tubes and their load-deflection curves

Table 4.2 shows the final failure load of various lay-ups tested and load at which first damage initiated. The first damage load was recorded when sound of crack was heard. The characteristics of the load-deflection curves of composite tubes and their strength are described below.

Table 4.2 Failure load and first damage load of tube specimens

Specimen Code	Lay-up (outer to inner layer)	R_i (inch)	Failure Load (lbs)		Average Load(lbs)	
			First Damage	Final Failure	1st	Final
2A1	$[0/-45/+45/+45/-45/0]_T$	0.375	180	275	197	290
			200	295		
			210	300		
2A2	$[-45/+45/0/-45/+45/0]_T$	0.375	200	330	217	367
			225	380		
			225	390		
2A3	$[0/0/-45/+45/-45/+45]_T$	0.375	180	315	190	317
			200	320		
2B1	$[0/-45/+45/+45/-45/0]_T$	0.250	140	200	150	208
			150	215		
			160	210		
2B2	$[0/-45/+45/+45/-45/0]_T$	0.500	110	300	117	325
			125	350		
2B3	$[0/-45/+45/+45/-45/0]_T$	0.950	125	350	128	367
			125	350		
			135	400		
2C1	$[0/-15/+15/+15/-15/0]_T$	0.375	190	215	193	220
			190	220		
			200	225		
2C2	$[0/-75/+75/+75/-75/0]_T$	0.375	150	280	162	310
			160	300		
			175	350		

4.2.1 Sudden failure of composite tubes

Figure 4.2 shows a typical load-displacement curve. As indicated, the curve is linear elastic to failure. No yielding is observed before total failure. This behavior was observed on specimens 2A1, 2A2, 2A3, 2B1 and 2C2. For these specimens, visual damage was not seen by naked eye until close to failure load. Fiber breaking and internal damage was heard with minor sounds at loads marked in Table 4.2 above.

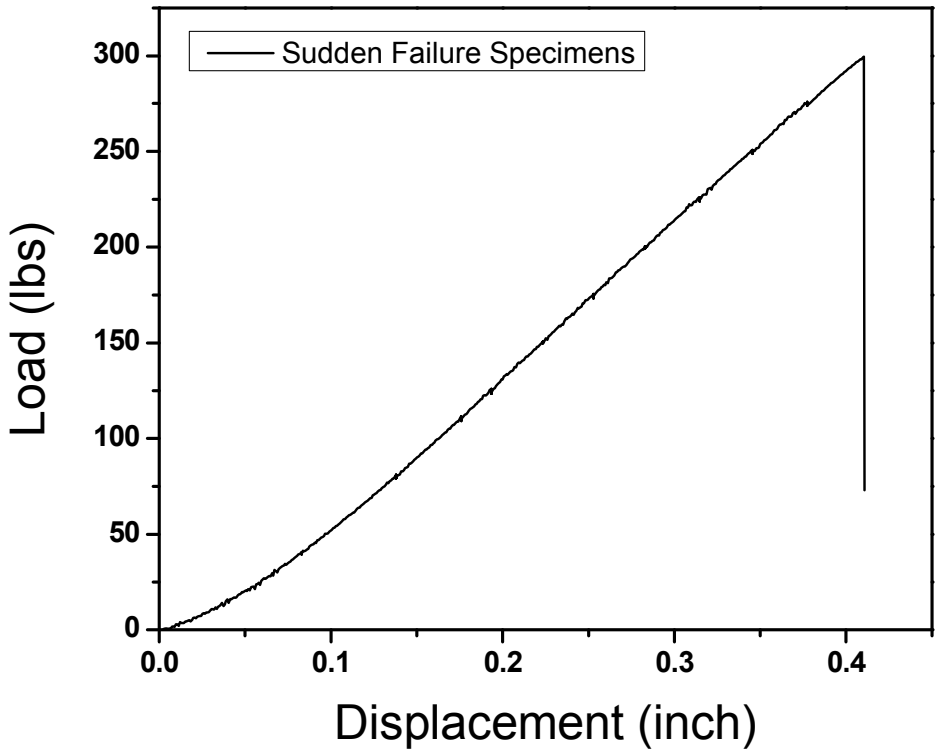

Figure 4.2 Load vs. Displacement for sudden failure specimens.

4.2.2 *Gradual failure of composite tubes*

Figure 4.3 shows load vs. displacement curve for tube specimens 2C1 that exhibited load drop. Specimens 2B2, 2B3 and 2C1 showed gradual load drop behavior before final failure. For the case of 2C1 specimens, the cross-section of tube remains almost circular after load drop. The significant load drop is due to damage occurring in 0˚ply and delamination at the interface of +15˚ and -15˚plies.

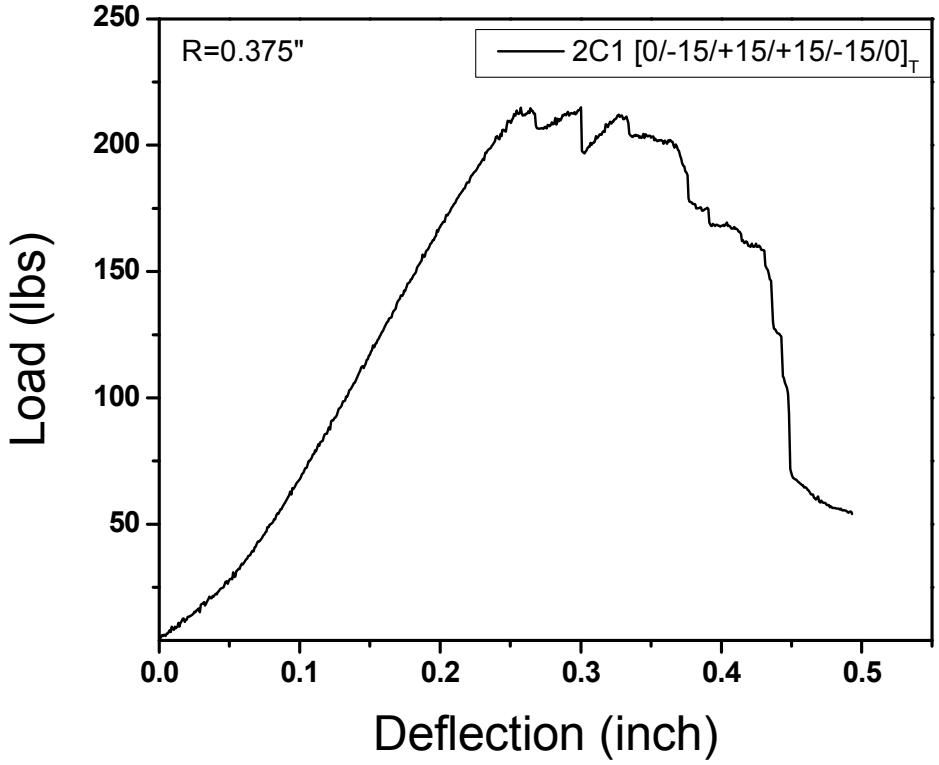

Figure 4.3 Load vs. Displacement for 2C1 specimen.

For the case of 2B2 and 2B3, change in the shape of tubular cross-section was prominent at much lower loads as compared to failure load. Due to large diameter, these

specimens were able to sustain high loads with less deflection. Figure 4.4 shows load-displacement curve for specimen 2B2.

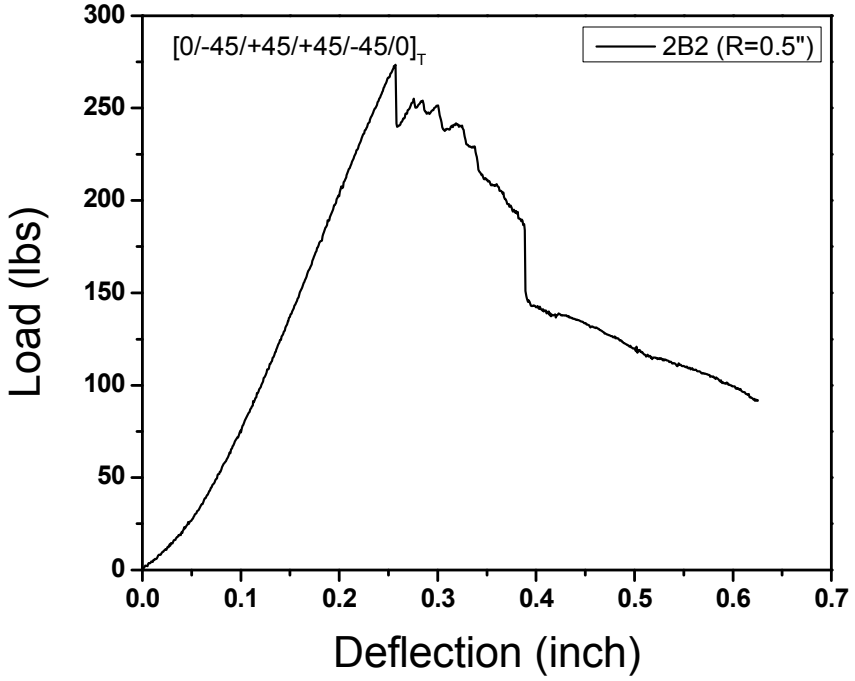

Figure 4.4 Load vs. Displacement for 2B2 specimen.

4.2.3 Effect of radius

Figure 4.5 shows load-deflection curves of tubes with various radii under bending. All of the tubes considered here have the identical lay-ups with radius ranging from 0.25 inches to 1.0 inches. As indicated, the strength of composite tube increases as its radius increases. Conversely, the deflection decreases as the tube radius increase. However, this is not the case for composite tube. For isotropic material, the strength of

the tube is proportional to the ratio of bending stiffness which is related to moment of inertia (I).

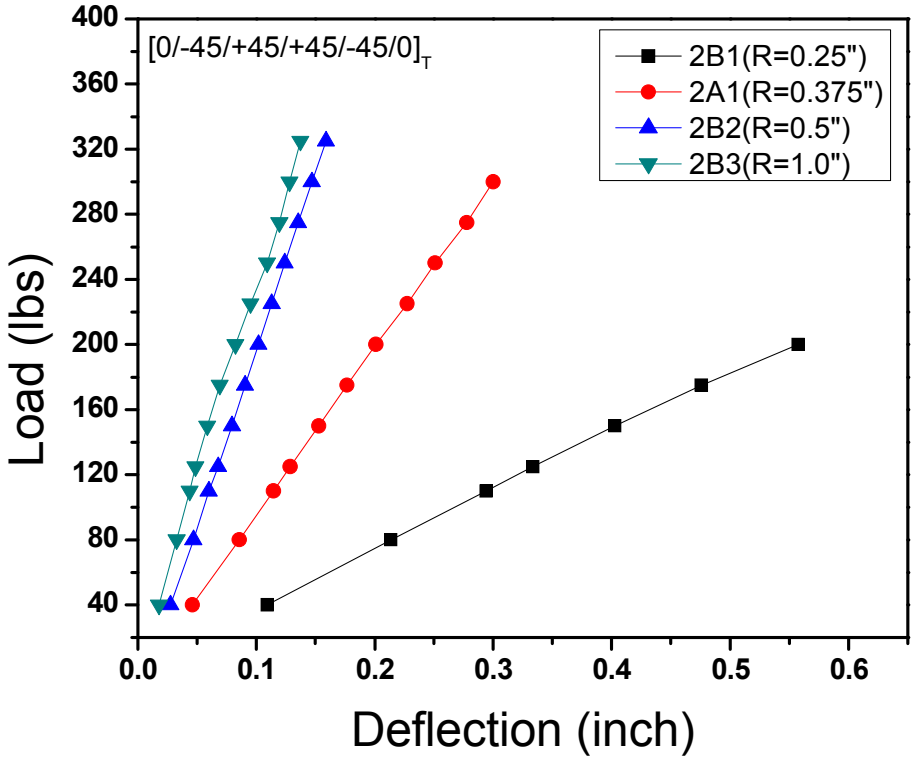

Figure 4.5 Deflection vs. Load curves for various inner radii.

4.2.4 Effect of 0˚ ply location

Figure 4.6 shows the comparison of the tube deflection for the position of 0˚ply in the tubular wall laminate. The results indicate that there is an insignificant difference in the slope of the load-deflection curve. This implies that the bending stiffness of the tube does not appear significant influence due to the change of the position of 0˚-ply. It is well known that placing 0˚ ply away from the mid-plane of the laminate gives higher

bending stiffness of the laminate. However, the bending stiffness of the laminate tube, shown in equation 3.8 constitutes two parts. One is due to the bending stiffness with respect to its mid-plane bending axis and the other part is from the axis shift. Examining the equation, we found the latter part of the bending stiffness is dominant since it is related to the extensional stiffness of the laminate, [A]. It is known that position of 0˚ply in laminate affects [D] matrix, not [A] matrix. Therefore, the bending stiffness of the tube is insignificant difference.

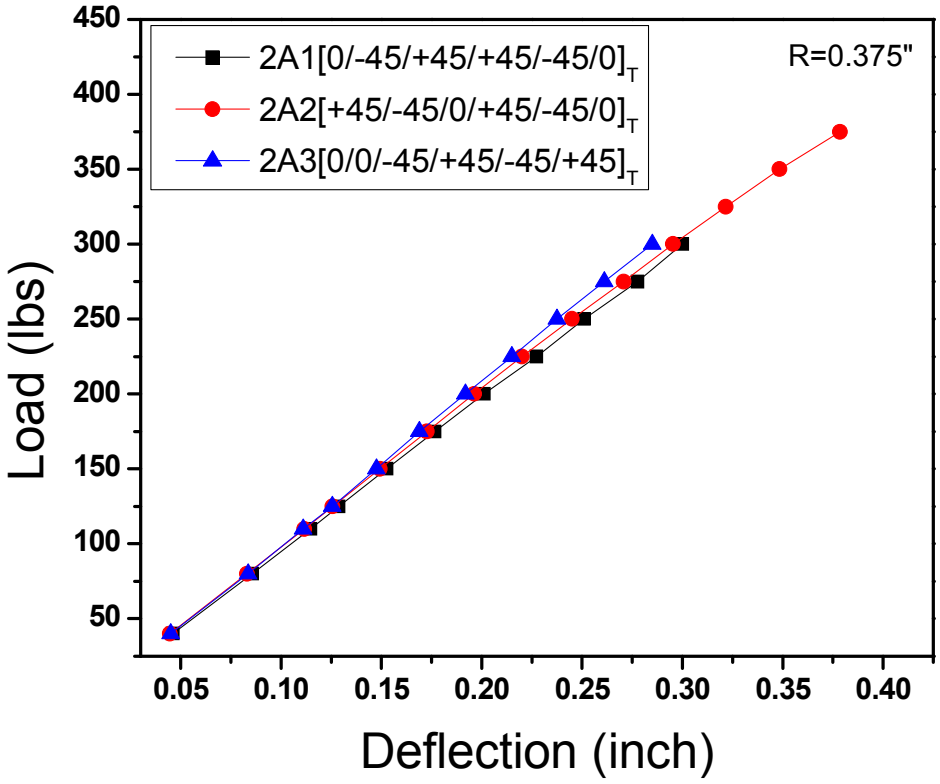

Figure 4.6 Deflection vs. Load data on number of zero-degree plies

4.2.5 Effect of fiber orientation of angle plies

Coupons with $\mp 75^{\circ}$, $\mp 45^{\circ}$ and $\mp 15^{\circ}$plies placed between two 0° plies in the wall laminates were used to study the effect of bending strength and the deflection. The load vs. deflection curves are shown in Figure 4.7. The results indicate that increasing fiber orientation of angle plies results in decrease of the bending stiffness but increase of the bending strength. The coupons with $\mp 75^{\circ}$ plies placed have the highest bending strength and the largest deflection of the tube among those coupons studied. Intuitively, the coupons with $\mp 15^{\circ}$ should carry the higher load to failure compared to the other two sets of coupons. Carefully examining the failure of the coupons, it is found that significant shear failure and delamination occurs at the interface of $-15^{\circ}/+15^{\circ}$ layers.

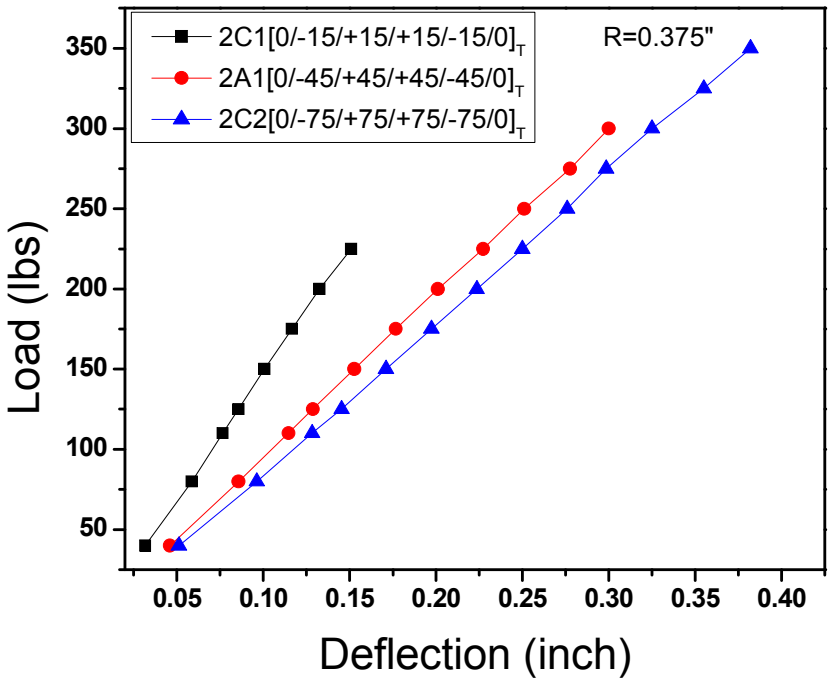

Figure 4.7 Effect of fiber orientation in symmetric lay-ups in Deflection vs. Load

4.3 Curvature effect on bending stiffness of composite tube

Bending stiffness of uniform circular tube with isotropic properties can be evaluated by 2D-model using solid mechanics equations. Laminated composites being transversely isotropic materials as discussed in chapter 3 need to be correctly evaluated using lamination theory. Table 4.3 shows the calculated bending stiffness based on both experimental methods and analytical methods described in chapter 3.

Table 4.3 Bending stiffness of various lay-ups of composite tubes

Lay-up	Dial-Gage Results	Plate Approach	Smear Approach	Strain Gage Results
2A1	4.553×10^4	5.611×10^4	5.98×10^4	5.779×10^4
2A2	4.645×10^4	5.604×10^4	5.975×10^4	5.715×10^4
2A3	4.709×10^4	5.602×10^4	5.973×10^4	6.22×10^4
2B1	1.721×10^4	1.866×10^4	1.99×10^4	1.86×10^4
2B2	8.702×10^4	1.488×10^5	1.586×10^5	none
2B3	1.206×10^5	7.84×10^5	8.358×10^5	none
2C1	6.634×10^4	1.142×10^5	1.16×10^5	1.243×10^5
2C2	4.092×10^4	4.877×10^4	5.154×10^4	5.032×10^4

4.3.1 Discussion for possible error in approaches

As seen in Table 4.3 above, bending stiffness for specimen 2B1 is closest match between experimental approach and plate approach. 2B1 has smallest outer diameter and hence change of cross-section from uniform circular to elliptical is minimal. In specimens 2A1, 2A2 and 2A3 outer radius is same with different stacking sequence. Bending stiffness calculated as per plate approach differs from experimentally calculated due to change of cross-section observed. Below is table 6 showing horizontal and vertical diameter data for some cases that confirm the change in shape from circular as assumed in plate approach model in chapter 3. 2B2 and 2B3 are the largest diameter

tubes and shape not just changed from uniform circular to elliptical but deformation mechanism was much more complicated as seen in Figure 4.8. In these specimens change of shape was localized as well and plate approach was not capable to determine it's bending stiffness.

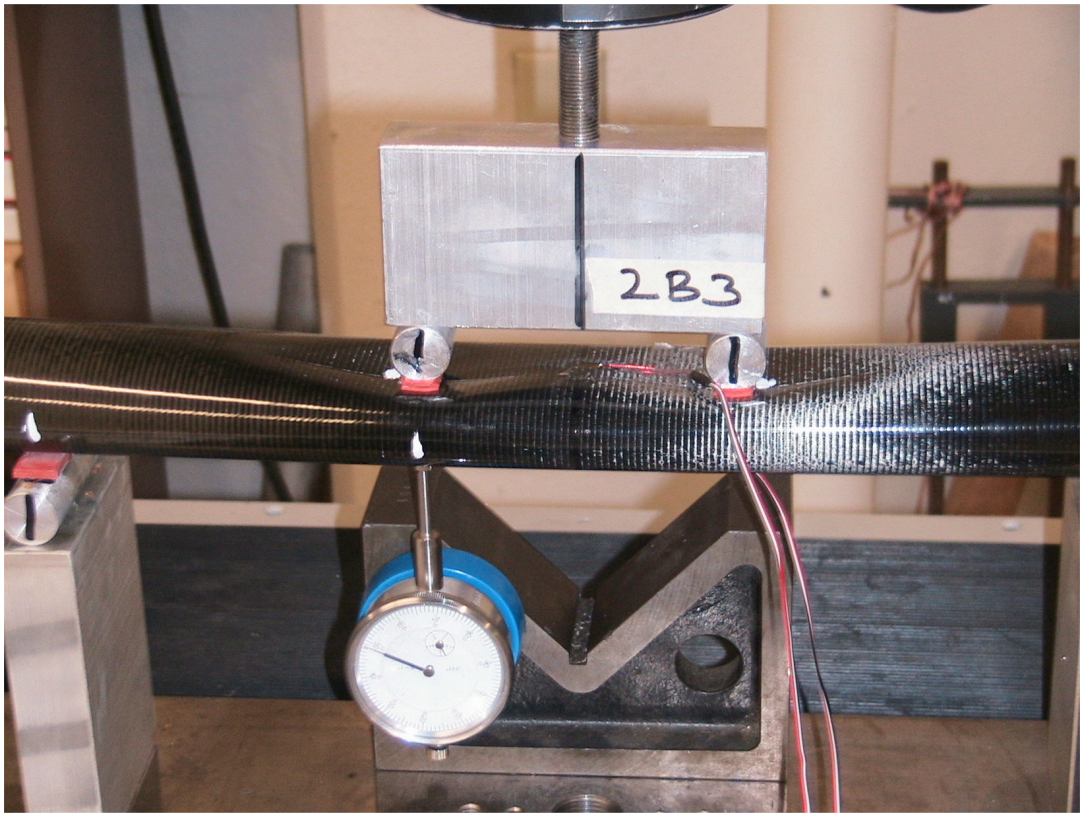

Figure 4.8 2B3 specimen under four-point bending.

CHAPTER 5

FAILURE INVESTIGATION

Failure analysis is an important tool used in to study their fracture behavior under loading and their physics behind the failure. Cause of failure is determined using fractography and an insight of failure mechanism can be obtained by using this tool. In study of any failure, broad spectrum of possibilities for the failure to occur must be carefully analyzed. Two failure inspection methods were often adopted. They are:

1. X-ray radiography
2. Optical Microscopy

In this chapter, we will discuss the failure of composite tube by using these two inspection methods.

5.1 Failure Process and X-ray Radiography

X-ray radiography is a non-destructive method for damage inspection. It was used to get basic information of the failure such as the size of the failure zone. Damage size was important information which needed to be addressed before the destructive method is conducted. In this technique, specimen preparation was important procedure to ensure successful results. Since the graphite/epoxy composite is transparent to x-ray, a solution opaque to x-ray embedded in the composite is needed to enhance the damage of the specimen. Zinc iodide was chosen for this matter to enhance damage size. The solution was diluted with distilled water.

5.1.1 X-ray radiographic procedure

1. The damage area of the composite tube specimens were soaked in the solution for approximately 20-30 minutes to ensure complete seepage of zinc iodide into the specimen.
2. Excess solution of zinc iodide on the specimen was removed by using clean lint free cloth or some other media.
3. Polaroid film (52-type) was placed below specimen on specified markings to get proper imaging of fracture region. This was critical step in getting relevant image.
4. Cabinet x-ray machine was used at a voltage of 12kV and specimens were exposed to x-rays for 10 minutes to generate results.
5. After the exposure voltage was turned down at slow rate to avoid element malfunctioning.
6. Film taken out is thus developed in the Polaroid film developer.

5.1.2 Analysis of x-ray images

Figure 5.1 through 5.3 shows the radiographs of 2A1, 2A2 and 2A3 specimens, respectively. These specimens have the same diameter but different stacking sequence (see Table 4.2). Specimens 2A1, 2A2 and 2A3 have one 0˚, none and two 0˚ plies on the outer surface of the wall laminate, respectively. The dark region shown in Figure 5.1 is where zinc iodide solution penetrated in cracks and illuminated it on the film. It is clearly seen that crack on the circumference is running around in slant fashion and is localized clearly around the loading point. This justifies presence of hidden possible

delamination as well. The cracks and delamination are in the inner layers and can't be viewed just using x-ray radiography and need to be opened up to view them at higher magnifications. This specimen failed at load around 300 lbs and no visual damage was seen until the end. Cracking sound was prominent after 220 lbs and dark black spot is the actual loading point in this specimen.

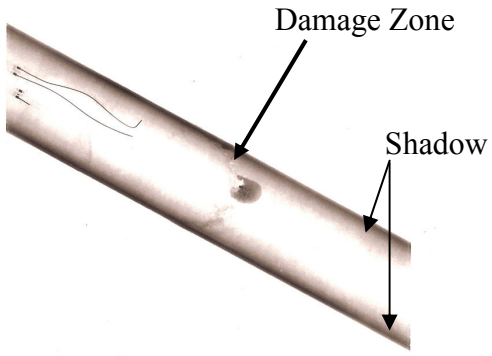

Figure 5.1 X-ray image of specimen 2A1.

Figure 5.2 is the image of specimen 2A2 and dark region shows the presence of visual crack after tube failed. This specimen sustained load until about 350 lbs and damage was again sudden as in previous case and we see in this one as well that crack started at the loading point and continued from layer to layer around the circumference of tube in slant fashion.

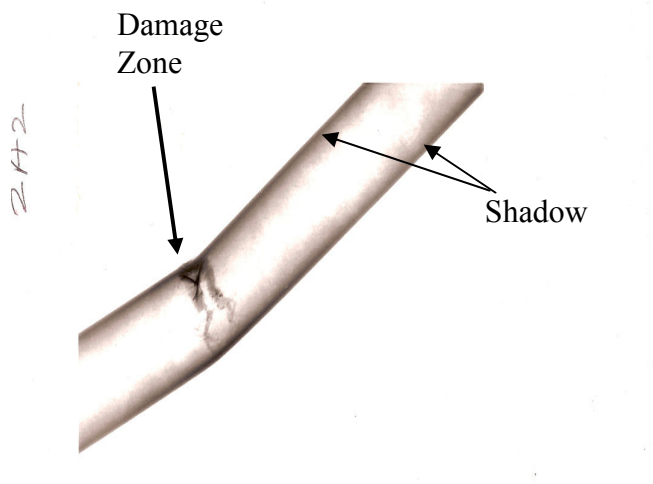

Figure 5.2 X-ray image of specimen 2A2.

In Figure 5.3, damage of specimen 2A3 was predominantly the same as the previous specimens shown. The crack is also observed to be from layer-to-layer in oblique manner indicating possibility of shear failure.

In viewing of the above three specimens, we observed that shear cracks are more pronounced in specimen 2A2. this is because of more ±45˚ plies and none 0˚ ply near the outer surface of the wall laminate.

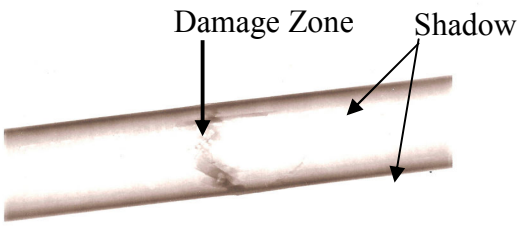

Figure 5.3 X-ray image of specimen 2A3.

Figure 5.4 is the same lay-up as 2A1 but with smaller diameter. Sudden failure and fiber bundles breakage was finally observed. Cracking sound was heard but not significantly loud. This suggests there are some matrix cracks and delamination occurring.

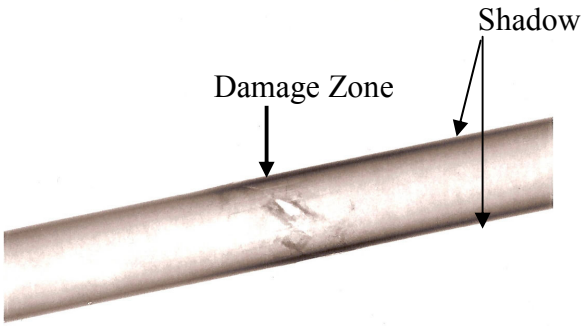

Figure 5.4 X-ray image of specimen 2B1.

In Figures 5.5 and 5.6, specimens 2B2 and 2B3, respectively, are the tubes with same lay-up as 2B1 but larger diameters. Large deformation was observed while the tube was loaded over 225 lbs and then the cross-section was no longer circular. The peak loads in both the cases was close to 350 lbs owing to change of shape involved and failure was not sudden and load drop was consistent from peak load to the point test stopped.

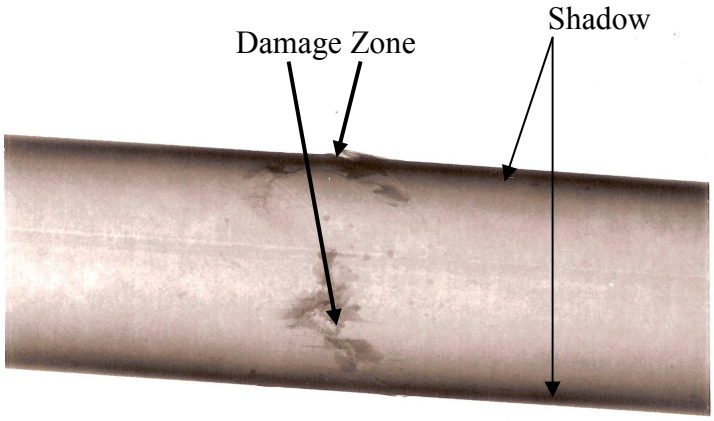

Figure 5.5 X-ray image of specimen 2B2.

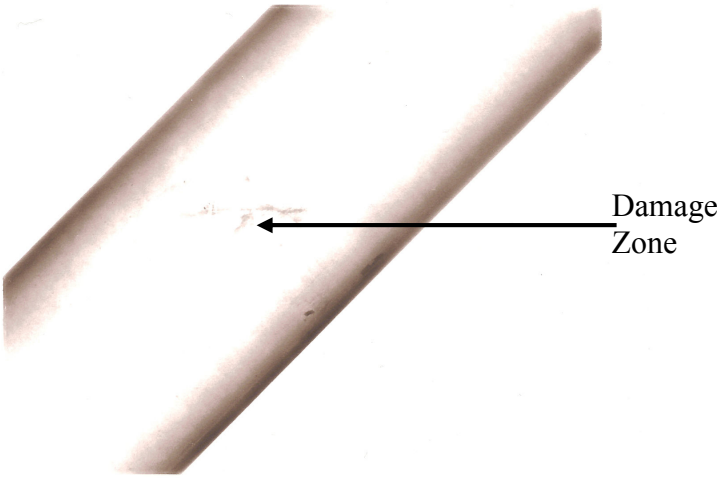

Figure 5.6 X-ray image of specimen 2B3.

Below is Figure 5.7 showing image of damage region in specimen 2C1. Crack in this case also initiated near the loading point and continued in shear fashion across the circumference. Failure in this case happened at load of 225 lbs and cracking sound started at approximately 200 lbs and sample failed with sudden quick tearing sound at 225 lbs.

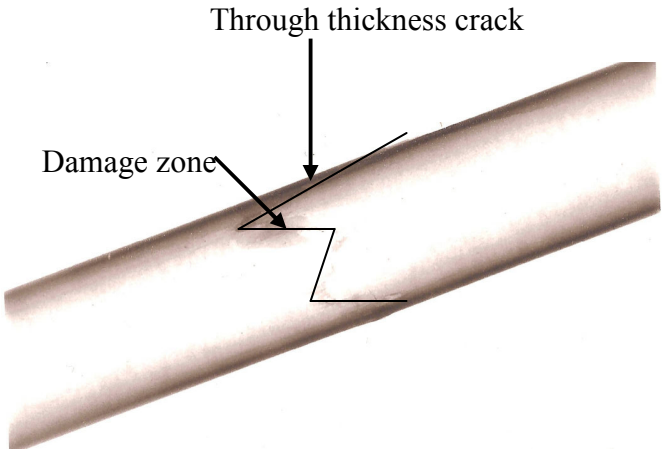

Figure 5.7 X-ray image of specimen 2C1.

In Figure 5.8, specimen 2C2 failed at load of 300 lbs with sudden failure and no significant cracking or tearing sound was heard in this case.

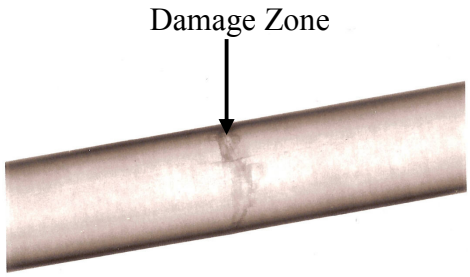

Figure 5.8 X-ray image of specimen 2C2.

5.2 Optical Microscopic Analysis

Analysis of x-ray radiography can not provide the detailed information of failure process, layer location of delamination. To meet this need, optical microscopy is used to obtain this information. Optical microscope with magnification between 50X-400X was used to investigate the fracture surface. For that purpose the failed tubes have to be cut at the specified location. The selection of location and cutting process are critical to

preserve fracture surface as well. Figure 5.9 shows the specimen taken from the tube for optical investigation. A procedure is discussed in the next section.

5.2.1 Experimental Procedure

1. Failed tube was marked for cutting locations and that was decided upon analysis from x-ray images.
2. The full-length tube was cut into small round piece containing fracture area to eliminate the size being barriers to further cut open the tubes.
3. Cut was made by using diamond-edged micro cutter to open the failed sample into two halves showing fracture on both halves and direction of cut was such chosen to have minimal or no effect on fracture area.
4. The opened specimen was then mounted on sample holder to firmly place it just below microscope to view it under low and then higher magnifications.

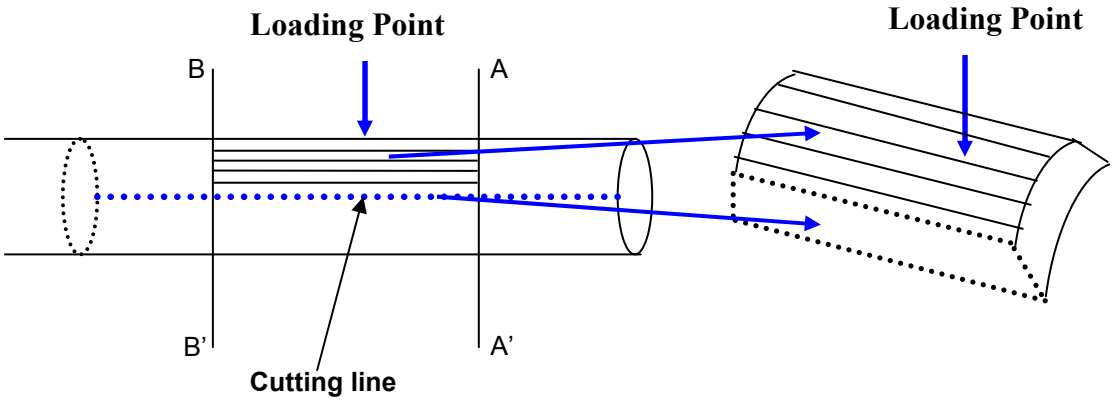

Figure 5.9 Specimen for Optical Microscopy investigation.

5.2.2 Delamination failure in tubes

Reinforcement in laminated composites is in the plane and none in the thickness direction. Hence, failure often occurs in between layers, namely delamination. Figure 5.10 shows the fractured specimen 2A1 which has 0˚ fibers in its innermost and outermost layers followed by symmetrically placing -45˚ and +45˚ fibers. Delaminations are observed at the interfaces between 0 and -45˚ layers and +45 and -45˚ layers of the innermost layers.

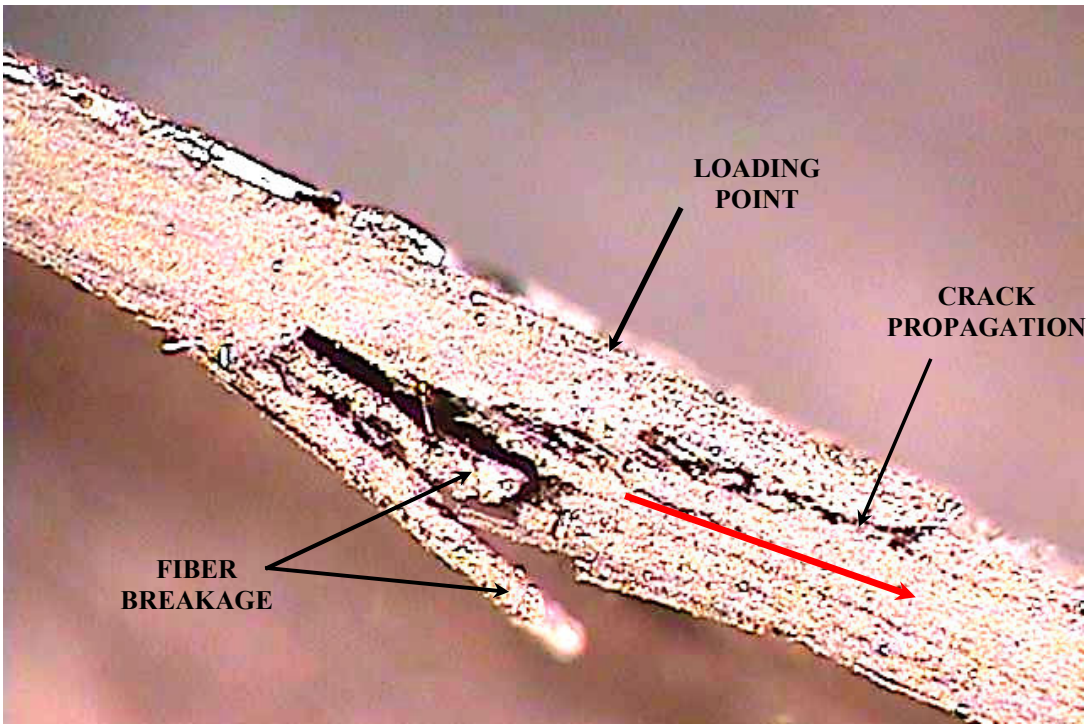

Figure 5.10 Fractured tube specimen 2A1 at 150X magnification

In the Figure 5.11, the fiber failures were occurred at the outermost layers of +45 and -45 plies and the innermost layers of 0˚ and 45˚ plies. The delamination is also observed at the interface of 0 and -45 plies on the mid-plane of the laminate.

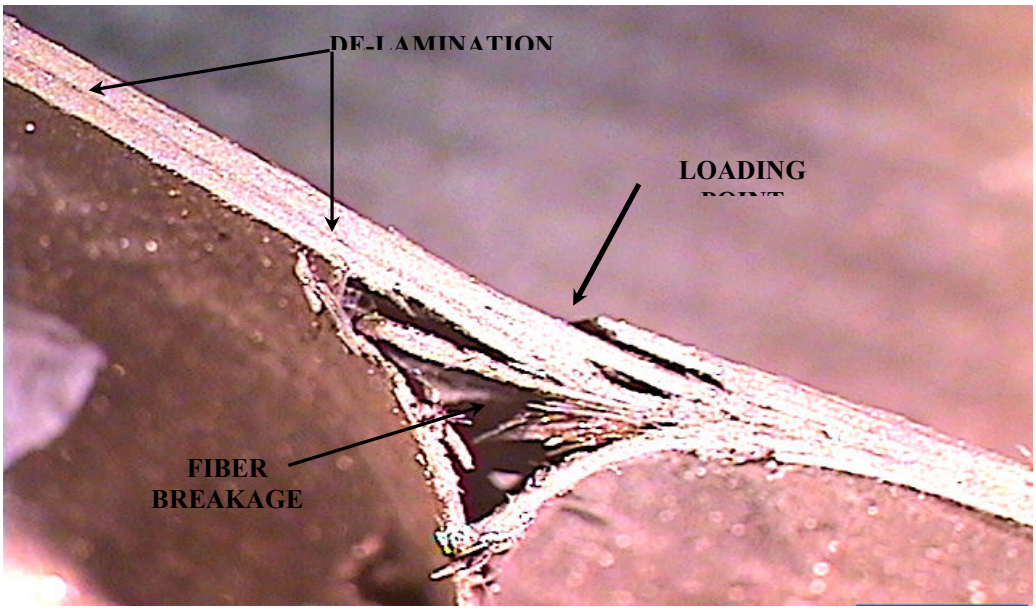

Figure 5.11 Fractured sample 2A2 at 70X magnification

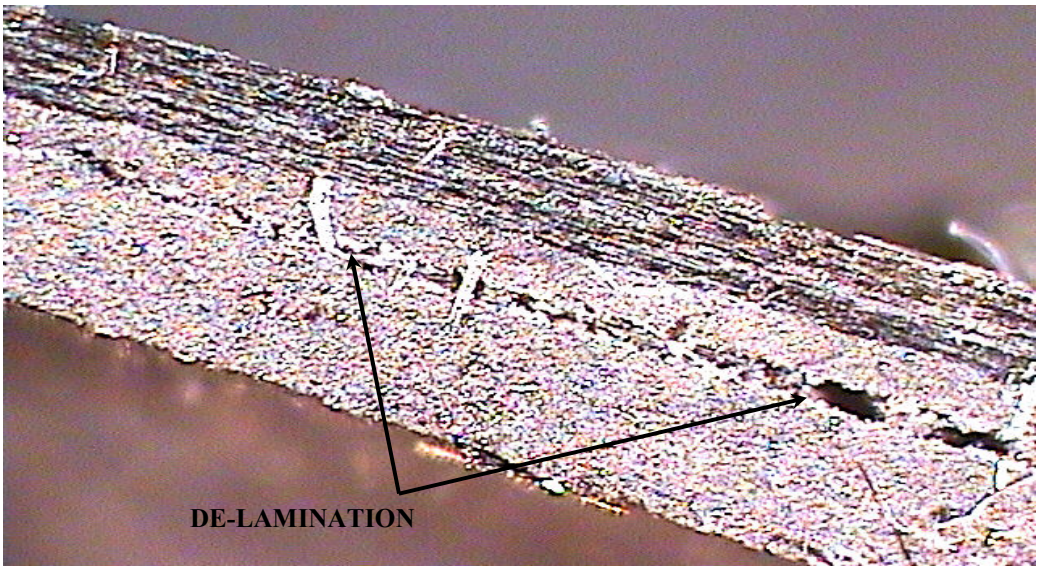

Figure 5.12 Fractured sample 2A3 at 350X magnification

Figure 5.12 shows the fracture image of specimen 2A3 which has all of 0˚ plies in the outermost layers. Delamination was observed in the mid-plane of the laminate.

In summary, for all of 2A1, 2A2 and 2A3 specimens, the delamination occurred mostly at the inner surface in the localized area near the loading point. Figure 5.13 and 5.14 shows extensive damage of fiber breakage and delamination for specimen 2A2 and 2A3, respectively. It should be noted that fracture surface shown is located at the mid plane of the entire tube where the highest shear occurs. Hence, the failure can be attributed to the shear failure.

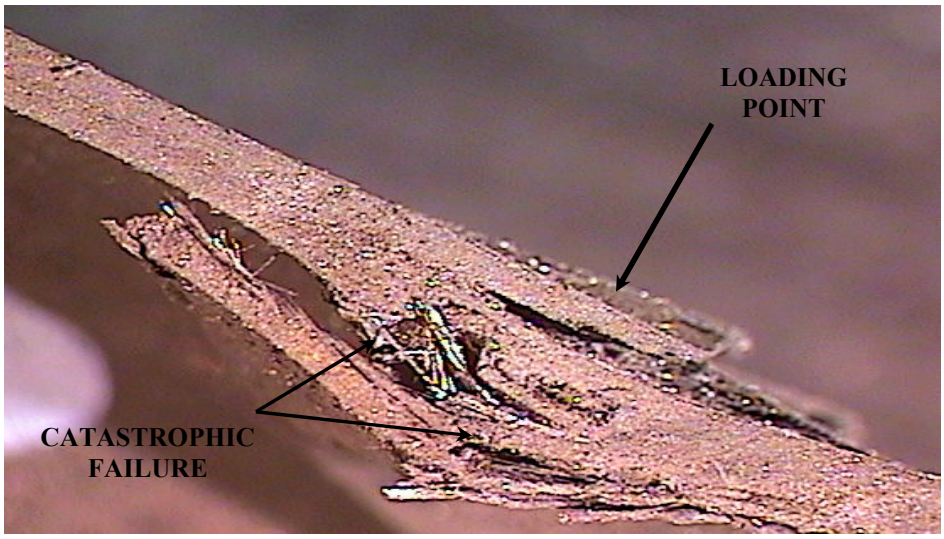

Figure 5.13 Specimen 2A2 at 100X magnification showing shear effect and failure between +45 and -45 plies

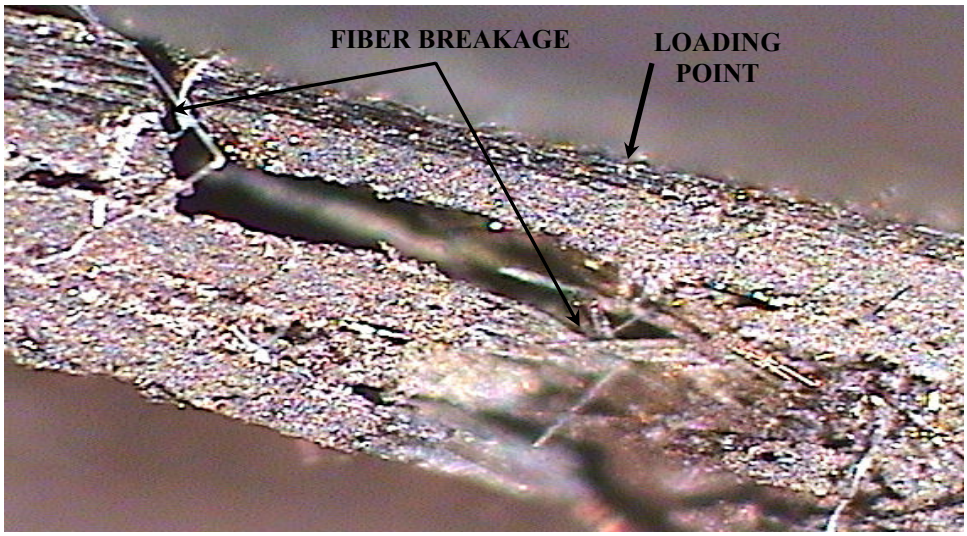

Figure 5.14 Specimen 2A3 at 300X magnification showing disastrous shear failure in the middle

Figure 5.15 and 5.16 shows that the crack initiates between the layers where the maximum shear mismatch (positive and negative shear), interface of +45 and -45 plies, but propagates in an oblique manner from layer to layer as well.

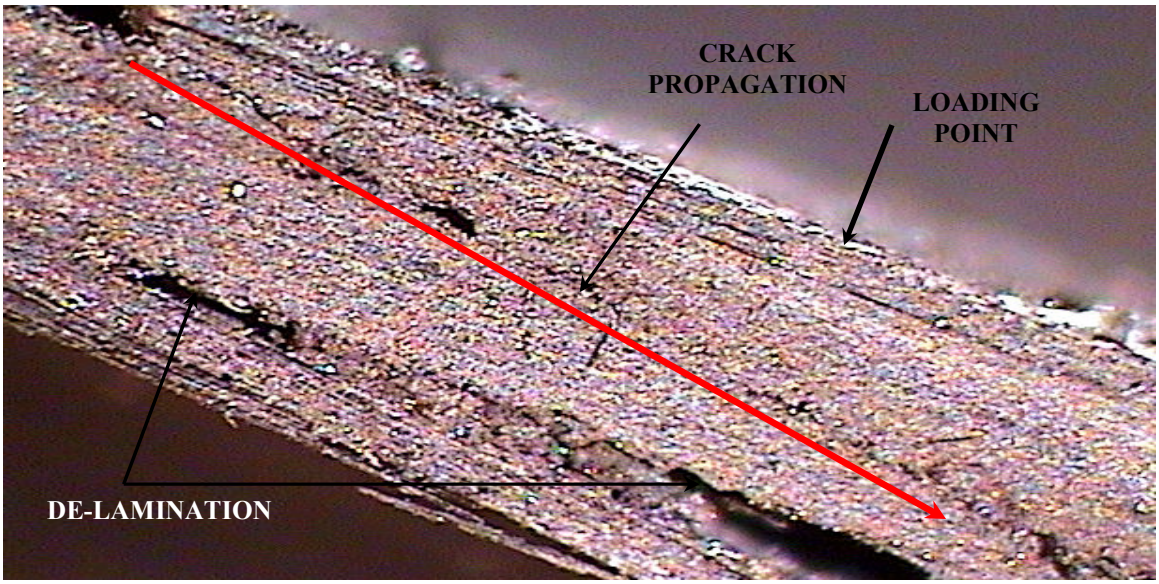

Figure 5.15 Specimen 2A1 at 275X showing delamination and crack propagation in oblique manner from layer to layer as well.

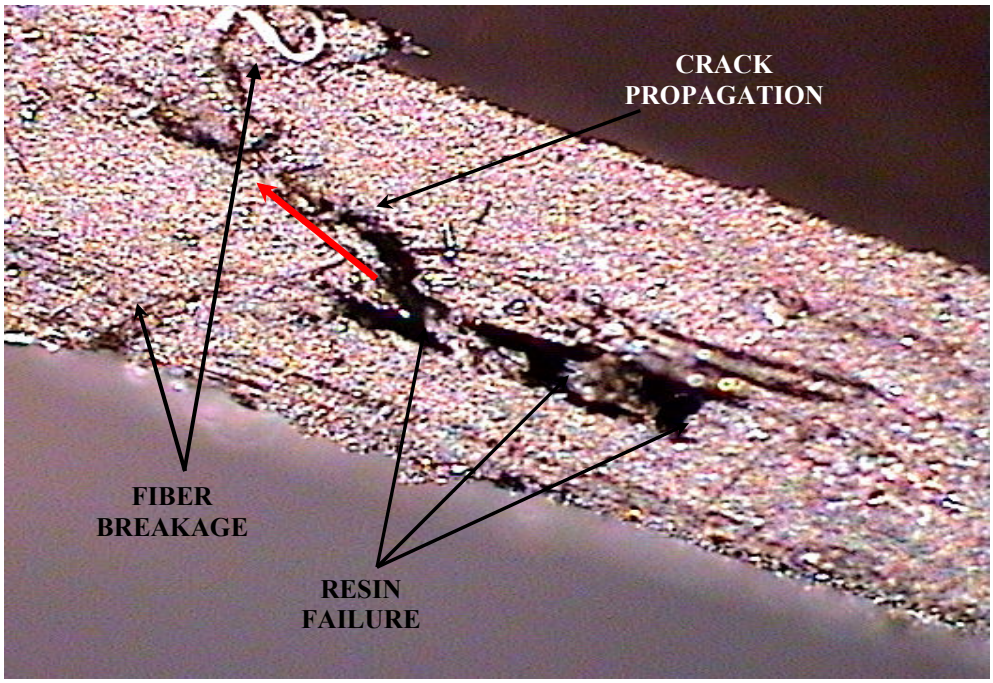

Figure 5.16 Crack propagation in 2A3 at 350X magnification.

Figure 5.17 shows specimen 2B1 symmetric laminate with smaller radius has similar failure process as in specimen 2A1.

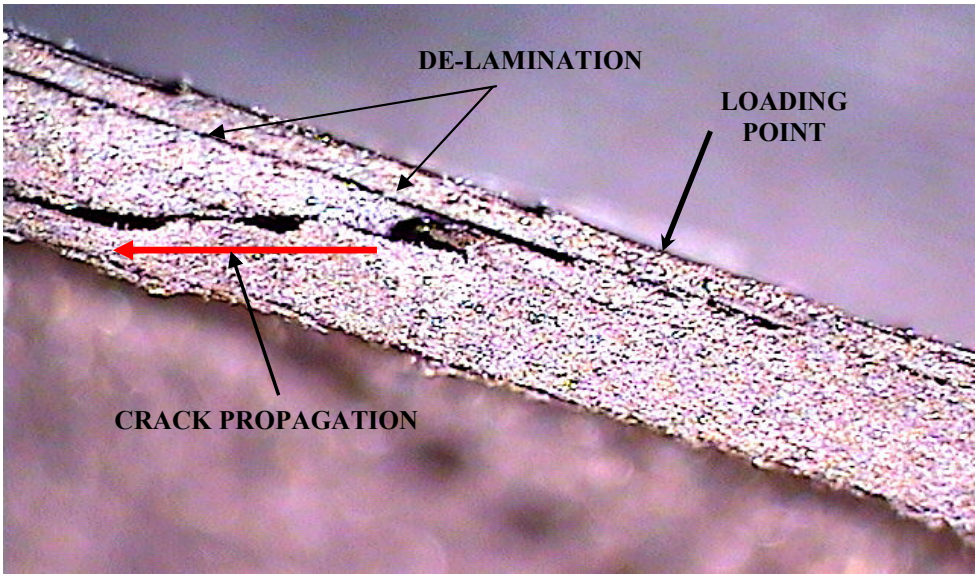

Figure 5.17 Failed sample 2B1 at 200X magnification showing crack propagation.

In the Figure 5.18 below is symmetric laminate with angle plies at +15˚ and -15˚ with 0˚ plies on outer most and innermost surface and delamination is observed in the -15 and +15 plies as that is the location where the highest shear mismatch occurs and crack tends to propagate from layer to layer as well in an oblique manner.

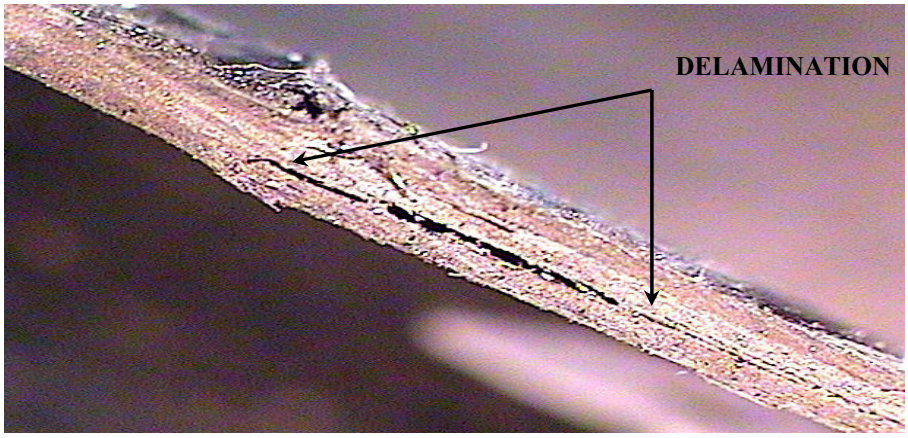

Figure 5.18 Failed sample 2C1 at 100X showing delamination and crack propagation from layer to layer as well.

CHAPTER 6

CONCLUSIONS

Four-point bending tests were conducted to evaluate the bending stiffness and strength on various sizes of the composite tubes. The walled laminates of the tubes with various stacking sequence of $[0/-45/+45/+45/-45/0]_T$ graphite/epoxy. Coupons of the material used for the tube were also tested to obtain the principal material properties.

Bending stiffness of the composite tube was calculated by analytical methods. Among analytical methods, both laminated plate method and smear property method were used. The bending stiffness of the tube was also calculated based upon the measurement data. Experimental bending stiffness is calculated from the longitudinal strains at both upper and bottom surface. It is also calculated from the dial gage readings.

From this study we found that:

- For all of the tube studied, bending stiffness obtained from laminated plate method is closer to the one obtained by strain gage data than from smear property method.
- The composite tube with smallest radius has least difference in bending stiffness obtained by laminated plate approach and experimental method for the tube with $[0/-45/+45/+45/-45/0]_T$ laminate.

- For large radius of the tubes, the experimental values of the bending stiffness deviate from the analytical prediction due to deformation in shape from circular cross-section to elliptical shape under load.
- Stacking sequence of tube walled laminate does not appear to affect the bending stiffness of composite tube, in particular for larger radius of the tubes.
- Bending strength of tubes with identical radius increases as the 0 layers in laminates are placed close to the mid-plane of the wall laminate.
- Unlike isotropic material, the bending stiffness of the tube is not proportional to R^4. It is a function of R^3 and R as well as the material property of the tube.
- Among the tubular walled laminates such as $[0/-15/+15/+15/-15/0]_{T,}$ $[0/-45/+45/+45/-45/0]_{T,}$ $[0/-75/+75/+75/-75/0]_T$, the tubes have the highest bending strength with $[0/-75/+75/+75/-75/0]_T$ laminate and have the lowest strength with $[0/-15/+15/+15/-15/0]_T$ laminate.

Fracture analysis was also conducted by using both x-ray radiography and optical microscopy to investigate the failure process of the tube under bending. No attempt was focus on identification of fracture modes because of catastrophic and multiple failures observed. The following observations were obtained during and after test:

- Damage is initiated at the loading point then propagates in the shear direction along the circumference.
- The final failure is in compression. No failure in the tension side of the tube is observed.
- The failure process depends on the fiber orientation and ply stacking sequence of the walled laminate of the tubes.
- Fiber breakage and delamination were observed as the prominent damage mode.

For a better estimate on bending stiffness of the composite tubes undergoing deformation in shape, closed form solution incorporating deformation of cross-section from circular to elliptical is needed. Future scope of this study can involve estimate of bending stiffness of tube specimens involving shape change by using modified model of plate approach.

APPENDIX A

MATHEMATICA CODE FOR STIFFNESS MATRICES

(*Closed form solution for stiffness matrices of composite tubes*)

E_1=20.0x10^6; E_2=1.77x10^6; G_{12}=1.1x10^6; υ_{12}=0.313; t_{ply}=0.0058;

$$\nu_{21} = \frac{E_2}{E_1}\nu_{12};$$

$$Q_{11} = \frac{E_1}{1-\nu_{12}.\nu_{21}};\ Q_{22} = \frac{E_2}{1-\nu_{12}.\nu_{21}};\ Q_{22} = Q_{21} = \frac{\nu_{12}E_2}{1-\nu_{12}.\nu_{21}};\ Q_{66} = G_{12};$$

h= Table [i, {i,-3, 3}] t_{ply};

$$\theta = \frac{\pi}{4}\{0,-1,+1,+1,-1,0\};$$

R=0.39;

$$\bar{A}_{11} = 2\pi R\left(\sum_{i=1}^{6}\left(\left(\left(Cos[\theta[[i]]]\right)^4 Q_{11} + \left(Sin[\theta[[i]]]\right)^2\left(Cos[\theta[[i]]]\right)^2\left(Q_{12}+2Q_{66}\right) + \frac{3}{8}\left(Sin[\theta[[i]]]\right)^4 Q_{22}\right)\left(h[[i+1]]-h[[i]]\right)\right)\right)$$

$$\bar{A}_{12} = 2\pi R\left(\sum_{i=1}^{6}\left(\left(\left(Sin[\theta[[i]]]\right)^2\left(Cos[\theta[[i]]]\right)^2\left(Q_{11}+\frac{3}{8}Q_{22}-2Q_{66}\right) + \frac{1}{2}\left(Cos[\theta[[i]]]\right)^4 + \left(Sin[\theta[[i]]]\right)^4 Q_{12}\right)\left(h[[i+1]]-h[[i]]\right)\right)\right)$$

$$\bar{A}_{22} = 2\pi R\left(\sum_{i=1}^{6}\left(\left(\left(Sin[\theta[[i]]]\right)^4 Q_{11} + \left(Sin[\theta[[i]]]\right)^2\left(Cos[\theta[[i]]]\right)^2\left(Q_{12}+2Q_{66}\right) + \frac{3}{8}\left(Cos[\theta[[i]]]\right)^4 Q_{22}\right)\left(h[[i+1]]-h[[i]]\right)\right)\right)$$

$$\bar{A}_{16} = 2\pi R\left(\sum_{i=1}^{6}\left(\left(\left(Sin[\theta[[i]]]\right)\left(Cos[\theta[[i]]]\right)^3\left(Q_{11}-\frac{1}{2}Q_{12}-Q_{66}\right) + \left(Sin[\theta[[i]]]\right)^3\left(Cos[\theta[[i]]]\right)\left(\frac{1}{2}Q_{12}-\frac{3}{8}Q_{22}+Q_{66}\right)\right)\left(h[[i+1]]-h[[i]]\right)\right)\right)$$

$$\bar{A}_{26} = 2\pi R\left(\sum_{i=1}^{6}\left(\left(\left(Sin[\theta[[i]]]\right)^3\left(Cos[\theta[[i]]]\right)\left(Q_{11}-\frac{1}{2}Q_{12}-Q_{66}\right) + \left(Sin[\theta[[i]]]\right)\left(Cos[\theta[[i]]]\right)^3\left(\frac{1}{2}Q_{12}-\frac{3}{8}Q_{22}+Q_{66}\right)\right)\left(h[[i+1]]-h[[i]]\right)\right)\right)$$

$$\bar{A}_{66} = 2\pi R\left(\sum_{i=1}^{6}\left(\left(\left(Sin[\theta[[i]]]\right)^2\left(Cos[\theta[[i]]]\right)^2\left(Q_{11}+\frac{3}{8}Q_{22}-Q_{12}-Q_{66}\right) + \frac{1}{2}\left(\left(Sin[\theta[[i]]]\right)^4 + \left(Cos[\theta[[i]]]\right)^4\right)Q_{66}\right)\left(h[[i+1]]-h[[i]]\right)\right)\right)$$

$$\overline{B}_{11}=\pi R\left(\sum_{i=1}^{6}\left(\left(Cos[\theta[[i]]]\right)^4 Q_{11}+\left(Sin[\theta[[i]]]\right)^2\left(Cos[\theta[[i]]]\right)^2\left(Q_{12}+2Q_{66}\right)+\frac{3}{8}\left(Sin[\theta[[i]]]\right)^4 Q_{22}\right)\left(\left(h[[i+1]]\right)^2-\left(h[[i]]\right)^2\right)\right)$$

$$\overline{B}_{12}=\pi R\left(\sum_{i=1}^{6}\left(\left(\left(Sin[\theta[[i]]]\right)^2\left(Cos[\theta[[i]]]\right)^2\left(Q_{11}+\frac{3}{8}Q_{22}-2Q_{66}\right)+\frac{1}{2}\left(Sin[\theta[[i]]]\right)^4+\left(Cos[\theta[[i]]]\right)^4 Q_{12}\right)\left(\left(h[[i+1]]\right)^2-\left(h[[i]]\right)^2\right)\right)\right)$$

$$\overline{B}_{22}=\pi R\left(\sum_{i=1}^{6}\left(\left(\left(Sin[\theta[[i]]]\right)^4 Q_{11}+\left(Sin[\theta[[i]]]\right)^2\left(Cos[\theta[[i]]]\right)^2\left(Q_{12}+2Q_{66}\right)+\frac{3}{8}\left(Cos[\theta[[i]]]\right)^4 Q_{22}\right)\left(\left(h[[i+1]]\right)^2-\left(h[[i]]\right)^2\right)\right)\right)$$

$$\overline{B}_{16}=\pi R\left(\sum_{i=1}^{6}\left(\left(\left(Sin[\theta[[i]]]\right)\left(Cos[\theta[[i]]]\right)^3\left(Q_{11}-\frac{1}{2}Q_{12}-Q_{66}\right)+\left(Sin[\theta[[i]]]\right)^3\left(Cos[\theta[[i]]]\right)\left(\frac{1}{2}Q_{12}-\frac{3}{8}Q_{22}+Q_{66}\right)\right)\left(\left(h[[i+1]]\right)^2-\left(h[[i]]\right)^2\right)\right)\right)$$

$$\overline{B}_{26}=\pi R\left(\sum_{i=1}^{6}\left(\left(\left(Sin[\theta[[i]]]\right)^3\left(Cos[\theta[[i]]]\right)\left(Q_{11}-\frac{1}{2}Q_{12}-Q_{66}\right)+\left(Sin[\theta[[i]]]\right)\left(Cos[\theta[[i]]]\right)^3\left(\frac{1}{2}Q_{12}-\frac{3}{8}Q_{22}+Q_{66}\right)\right)\left(\left(h[[i+1]]\right)^2-\left(h[[i]]\right)^2\right)\right)\right)$$

$$\overline{B}_{66}=\pi R\left(\sum_{i=1}^{6}\left(\left(\left(Sin[\theta[[i]]]\right)^2\left(Cos[\theta[[i]]]\right)^2\left(Q_{11}+\frac{3}{8}Q_{22}-Q_{12}-Q_{66}\right)+\frac{1}{2}\left(\left(Sin[\theta[[i]]]\right)^4+\left(Cos[\theta[[i]]]\right)^4\right)Q_{66}\right)\left(\left(h[[i+1]]\right)^2-\left(h[[i]]\right)^2\right)\right)\right)$$

$$\overline{D}_{11}=\frac{2\pi R}{3}\left(\sum_{i=1}^{6}\left(\left(\left(Cos[\theta[[i]]]\right)^4 Q_{11}+\left(Sin[\theta[[i]]]\right)^2\left(Cos[\theta[[i]]]\right)^2\left(Q_{12}+2Q_{66}\right)+\frac{3}{8}\left(Sin[\theta[[i]]]\right)^4 Q_{22}\right)\left(\left(h[[i+1]]\right)^3-\left(h[[i]]\right)^3\right)\right)\right)$$
$$+2\pi R^3\left(\sum_{i=1}^{6}\left(\left(\frac{1}{2}\left(Cos[\theta[[i]]]\right)^4 Q_{11}+\frac{3}{4}\left(Sin[\theta[[i]]]\right)^2\left(Cos[\theta[[i]]]\right)^2\left(Q_{12}+2Q_{66}\right)+\frac{5}{16}\left(Sin[\theta[[i]]]\right)^4 Q_{22}\right)\left(h[[i+1]]-h[[i]]\right)\right)\right)$$

$$\overline{D}_{12}=\frac{2\pi R}{3}\left(\sum_{i=1}^{6}\left(\left(Sin[\theta[[i]]]\right)^2\left(Cos[\theta[[i]]]\right)^2\left(Q_{11}+\frac{3}{8}Q_{22}-2Q_{66}\right)+\frac{1}{2}\left(\left(Sin[\theta[[i]]]\right)^4+\left(Cos[\theta[[i]]]\right)^4\right)Q_{12}\right)\left(\left(h[[i+1]]\right)^3-\left(h[i]\right)^3\right)\right)$$
$$+2\pi R^3\left(\sum_{i=1}^{6}\left(\left(Sin[\theta[[i]]]\right)^2\left(Cos[\theta[[i]]]\right)^2\left(\frac{1}{2}Q_{11}+\frac{5}{16}Q_{22}-\frac{3}{2}Q_{66}\right)+\frac{3}{8}\left(\left(Sin[\theta[[i]]]\right)^4+\left(Cos[\theta[[i]]]\right)^4\right)Q_{12}\right)\left(\left(h[[i+1]]\right)-\left(h[[i]]\right)\right)\right)$$

$$\overline{D}_{22}=\frac{2\pi R}{3}\left(\sum_{i=1}^{6}\left(\left(\left(Sin[\theta[[i]]]\right)^4 Q_{11}+\left(Sin[\theta[[i]]]\right)^2\left(Cos[\theta[[i]]]\right)^2\left(Q_{12}+2Q_{66}\right)+\frac{3}{8}\left(Cos[\theta[[i]]]\right)^4 Q_{22}\right)\left(\left(h[[i+1]]\right)^3-\left(h[[i]]\right)^3\right)\right)\right)$$
$$+2\pi R^3\left(\sum_{i=1}^{6}\left(\left(\frac{1}{2}\left(Sin[\theta[[i]]]\right)^4 Q_{11}+\frac{3}{4}\left(Sin[\theta[[i]]]\right)^2\left(Cos[\theta[[i]]]\right)^2\left(Q_{12}+2Q_{66}\right)+\frac{5}{16}\left(Cos[\theta[[i]]]\right)^4 Q_{22}\right)\left(\left(h[[i+1]]\right)-\left(h[[i]]\right)\right)\right)\right)$$

$$\overline{D}_{16} = \frac{2\pi R}{3}\left(\sum_{i=1}^{6}\left(\left(Sin[\theta[[i]]](Cos[\theta[[i]]])^3\left(Q_{11}-\frac{1}{2}Q_{12}-Q_{66}\right)+(Sin[\theta[[i]]])^3(Cos[\theta[[i]]])\left(\frac{1}{2}Q_{12}-\frac{3}{8}Q_{22}-Q_{66}\right)\right)\left((h[[i+1]])^3-(h[[i]])^3\right)\right)\right)$$
$$+2\pi R^3\left(\sum_{i=1}^{6}\left(\left(Sin[\theta[[i]]](Cos[\theta[[i]]])^3\left(\frac{1}{2}Q_{11}-\frac{3}{8}Q_{12}-\frac{3}{4}Q_{66}\right)+(Sin[\theta[[i]]])^3(Cos[\theta[[i]]])\left(\frac{3}{8}Q_{12}-\frac{5}{16}Q_{22}+\frac{3}{4}Q_{66}\right)\right)\left((h[[i+1]])-(h[[i]])\right)\right)\right)$$

$$\overline{D}_{26} = \frac{2\pi R}{3}\left(\sum_{i=1}^{6}\left(\left(Cos[\theta[[i]]](Sin[\theta[[i]]])^3\left(Q_{11}-\frac{1}{2}Q_{12}-Q_{66}\right)+(Cos[\theta[[i]]])^3(Sin[\theta[[i]]])\left(\frac{1}{2}Q_{12}-\frac{3}{8}Q_{22}-Q_{66}\right)\right)\left((h[[i+1]])^3-(h[[i]])^3\right)\right)\right)$$
$$+2\pi R^3\left(\sum_{i=1}^{6}\left(\left(Cos[\theta[[i]]](Sin[\theta[[i]]])^3\left(\frac{1}{2}Q_{11}-\frac{3}{8}Q_{12}-\frac{3}{4}Q_{66}\right)+(Cos[\theta[[i]]])^3(Sin[\theta[[i]]])\left(\frac{3}{8}Q_{12}-\frac{5}{16}Q_{22}+\frac{3}{4}Q_{66}\right)\right)\left((h[[i+1]])-(h[[i]])\right)\right)\right)$$

$$\overline{D}_{66} = \frac{2\pi R}{3}\left(\sum_{i=1}^{6}\left(\left((Sine[\theta[[i]]])^2(Cos[\theta[[i]]])^2\left(Q_{11}+\frac{3}{8}Q_{22}-Q_{12}-Q_{66}\right)+\frac{1}{2}\left((Sin[\theta[[i]]])^4+(Cos[\theta[[i]]])^4\right)Q_{66}\right)\left((h[[i+1]])^3-(h[[i]])^3\right)\right)\right)$$
$$+2\pi R^3\left(\sum_{i=1}^{6}\left(\left((Sin[\theta[[i]]])^2(Cos[\theta[[i]]])^2\left(\frac{1}{2}Q_{11}+\frac{5}{16}Q_{22}-\frac{3}{4}Q_{12}-\frac{3}{4}Q_{66}\right)+\frac{3}{8}\left((Sin[\theta[[i]]])^4+(Cos[\theta[[i]]])^4\right)Q_{66}\right)\left((h[[i+1]])-(h[[i]])\right)\right)\right)$$

$$ABD = \left\{\left\{\overline{A}_{11},\overline{A}_{12},\overline{A}_{16},\overline{B}_{11},\overline{B}_{12},\overline{B}_{16}\right\},\left\{\overline{A}_{12},\overline{A}_{22},\overline{A}_{26},\overline{B}_{12},\overline{B}_{22},\overline{B}_{26}\right\},\left\{\overline{A}_{16},\overline{A}_{26},\overline{A}_{66},\overline{B}_{16},\overline{B}_{26},\overline{B}_{66}\right\},\left\{\overline{B}_{11},\overline{B}_{12},\overline{B}_{16},\overline{D}_{11},\overline{D}_{12},\overline{D}_{16}\right\},\left\{\overline{B}_{12},\overline{B}_{22},\overline{B}_{26},\overline{D}_{12},\overline{D}_{22},\overline{D}_{26}\right\},\left\{\overline{B}_{16},\overline{B}_{26},\overline{B}_{66},\overline{D}_{16},\overline{D}_{26},\overline{D}_{66}\right\}\right\}$$

Comp = Inverse [ABD];
Print [“ Resultant ABBD matrix”]
Comp // MatrixForm

“Bending Stiffness”
BS = 1/comp[[4]][[4]]

REFERENCES

1. Peters, S.T (1998). Chapter 49 of *Handbook of composites* (2nd edition). p.1044 Chapman and Hall

2. Fam, A.Z. and Rizkalla, S.H, "Flexural behavior of concrete-filled fiber-reinforced polymer circular tubes," *Journal of composites for construction*, Vol. 6, No.2, May 2002, pp.123-132.

3. Reddy, E.S and Binienda, W.K., "Prediction of crack initiation in unidirectional composite beams subject to four-point bending," *Composites Engineering*, Vol. 4, No. 7, 1994, pp.703-714.

4. Han, H., Taheri, F., Pegg, N. and Lu, Y, "A numerical study on the axial crushing of hybrid pultruded and ±45˚braided tubes," *Composite structures*, Volume 80, Issue 2, September 2007, pp.253-264.

5. Chan, W.S. and Demirhan, K.C, "A simple closed-form solution of bending stiffness for laminated composite tubes," *Journal of reinforced plastics and composites*, Vol. 19, No. 4, 2000, pp.278-291.

6. Hu, G., Bai, J., Demianouchko, E. and Bompard P, "Mechanical behavior of ±55˚Filament-Wound Glass-Fibre/Epoxy-Resin Tubes-III. Micromechanical model of the macroscopic behavior of tubular structures with damage and failure envelope prediction," *Composites Science and Technology*, 58 (1998), pp.19-29.

7. Stockwell, A. E. and Cooper, P. A, "Collapse of composite tubes under end moments," *AIAA-92-2389-CP*.

8. Padmanabhan, R, Macdonald, B.J and Hashmi, M.S.J, "Mechanical behavior of SiC reinforced aluminum thin walled tube under combined axial and torsional loading," *Journal of Materials Processing Technology*, Volumes 155-156, November 2004, pp.1760-1763.

9. Grediac, M., Pierron, F. and Zhavoronok, S, "Identification of the through-thickness properties of thick laminated tubes using virtual fields method," *International Journal of Solids and Structures*, Volume 37, Issue 32, 8 August 2000, pp.4437-4453.

10. Ellyin, F. and Maser, R, "Environmental effects on the mechanical properties of glass-fiber epoxy composite tubular specimens," *Composite Science and Technology*, Volume 64, Issue 12, September 2004,pp. 1863-1874.

11. Nixon, Mark W, "Extension-Twist Coupling of Composite Circular Tubes with Application to Tilt Rotor Blade Design," *AIAA/ASME/ASCE/AHS 28th Structures, Structural Dynamics and Materials Conference.* Pp 295-303.

12. Chen, G-S, Bidinger, G.M, Lou, M.C, "Impact Damage Tolerance of Thin Wall Composite Struts," *AIAA-93-1398-CP*.

13. Krafchak, T.M, Petra, J-M, Davidson, B.D, Chen, G-S, "Effect of Impact Damage on the Compression Fatigue Behavior of Composite Tubes," *AIAA-93-1399-CP*.

14. Jensen, David W, Pickenheim, Timothy R, "Compressive Behavior of Undulations in Filament-Wound Composites," *AIAA-9-1516-CP*.

BIOGRAPHICAL INFORMATION

Puneet Saggar was born on June 02, 1979 in India. He came to The University of Texas at Arlington in fall of 2004 after he took transfer from San Jose State University in California. He first took his composite courses with Dr. Wen S. Chan in spring of 2005 and upon showing his interest to work in the field of structural composites; Dr. Wen S. Chan took him as his student. He showed dedication and hard work towards completion of this study and endeavors to be a Materials Engineer working in the field of composite materials used in structures.